GEOPHYSICS, VOL. 79, NO. 6 (NOVEMBER-DECEMBER 2014); P. E353–E375, 16 FIGS., 8 TABLES.
10.1190/GEO2013-0347.1

Downloaded 11/18/14 to 138.67.11.98. Redistribution subject to SEG license or copyright; see Terms of Use at http://library.seg.org/

Spectral induced polarization of clay-sand mixtures: Experiments and modeling

Gonca Okay[1], Phillipe Leroy[2], Ahmad Ghorbani[3], Phillipe Cosenza[4], Christian Camerlynck[5], Justo Cabrera[6], Nicolas Florsch[7], and André Revil[8]

ABSTRACT

Spectral induced polarization or complex conductivity is a promising electric method in hydrogeophysics because of its sensitivity to water saturation, permeability, and particle size distribution (PSD). However, the physical and chemical mechanisms that generate the low-frequency complex conductivity of clays are still debated. To explain these mechanisms, the complex conductivity of kaolinite, smectite, and clay-sand mixtures was measured in the frequency range 1.4 mHz–12 kHz with various clay contents (100%, 20%, 5%, and 1% in volume of the clay-sand mixture) and salinities (distilled water, 0.1 $\mathrm{g\,L^{-1}}$, 1 $\mathrm{g\,L^{-1}}$, and 10 $\mathrm{g\,L^{-1}}$ of NaCl in solution). The results indicated the strong impact of the cation exchange capacity of smectite upon the complex conductivity of the material. The quadrature conductivity increased steadily with the clay content and was fairly independent of the pore fluid salinity. A mechanistic induced polarization model was also developed. It combined a Donnan equilibrium model of the surface electrochemical properties of clays and sand, a conduction model of the Stern and diffuse layers, a polarization model of the Stern layer, and a macroscopic conductivity model based on the differential effective medium theory. It also included the effect of the PSD. Our complex conductivity model predicted very well the experimental data, except for very low frequencies (<0.1 Hz) at which membrane polarization may dominate the observed response.

INTRODUCTION

Induced polarization is an extension to the classical direct current (DC) resistivity method and has become increasingly popular for hydrogeologic (Binley et al., 2005; Slater et al., 2010) and environmental applications (Holland et al., 2010), for instance, to estimate the low hydraulic conductivity of clayey materials acting as permeability barriers in landfills or in radioactive waste repositories (Weller and Börner, 1996; Lesmes and Friedman, 2005; Jougnot et al., 2010; Gazoty et al., 2012; Revil et al., 2013a, 2013b).

In saturated porous media, application of an alternating electric field results in electric conduction (electromigration of charge carriers, e.g., Waxman and Smits, 1968) and polarization processes. These processes are related to the (reversible) accumulation of electric charges at polarization length scales existing in the porous material (e.g., Vinegar and Waxman, 1984; Schön, 2004; Weller et al., 2013). These conductive and capacitive properties are controlled by various textural parameters of the porous medium including the clay content and mineralogy, specific surface area, and the grain or pore size distribution as well as electrochemical parameters such as the surface charge density or alternatively the cation

---

Manuscript received by the Editor 16 September 2013; revised manuscript received 15 July 2014; published online 11 November 2014.
[1]Hacettepe University, Department of Geomatics Engineering, Ankara, Turkey. E-mail: goncaokayahi@gmail.com.
[2]French Geological Survey, D3E Division, BRGM, Orléans, France. E-mail: p.leroy@brgm.fr.
[3]Yazd University, Department of Mining and Metallurgy, Yazd, Iran. E-mail: aghorbani@yazduni.ac.ir.
[4]University of Poitiers, CNRS, UMR 7285 IC2MP- HydrASA, ENSIP, Poitiers, France. E-mail: philippe.cosenza@univ-poitiers.fr.
[5]Sorbonne Universités, UPMC Univ Paris 06, UMR 7619 METIS, Paris, France. E-mail: christian.camerlynck@upmc.fr.
[6]French Institute of Radioprotection and Nuclear Safety, Fontenay-aux-Roses, France. E-mail: justo.cabrera@irsn.fr.
[7]Sorbonne Universités, UPMC Univ Paris 06, UMI 209 UMMISCO, Paris, France and CNRS, UMR 7619 METIS, Paris, France. E-mail: n.florsch@gmail.com.
[8]Colorado School of Mines, Department of Geophysics, Golden, Colorado, USA and ISTerre, Université de Savoie, Equipe Géophysique des Volcans, CNRS, UMR 5559, Bourget-du-Lac, France. E-mail: arevil@mines.edu .
© 2014 Society of Exploration Geophysicists. All rights reserved.

Downloaded 11/18/14 to 138.67.11.98. Redistribution subject to SEG license or copyright; see Terms of Use at http://library.seg.org/

exchange capacity (CEC) of the material, and the pore fluid chemical composition (Vacquier et al., 1957; Marshall and Madden, 1959; Vinegar and Waxman, 1984; Telford et al., 1990; Revil, 2013; Revil et al., 2013a, 2013b).

The goal of our study is to better understand the influence of the clay content, clay mineralogy, and pore water salinity upon complex conductivity measurements of water-saturated unconsolidated clays and clay-sand mixtures in the frequency range of 1.4 mHz–12 kHz. Our paper is divided into two main parts. The first part deals with the establishment of a new database of experimental results for the low-frequency complex conductivity of kaolinite and smectite. The second part deals with a comparison between this database and the predictions of a mechanistic induced polarization model, which considers the electrochemical conduction and polarization of the Stern layer around the particles.

BACKGROUND

The impact of clays on the induced polarization response of porous materials had been investigated, for instance, by Vacquier et al. (1957), Marshall and Madden (1959), Vinegar and Waxman (1984), and Telford et al. (1990). Their results indicate a significant increase of polarization in the presence of disseminated clays. Klein and Sill (1982) also confirm the importance of the clay mineralogy and pore water chemical composition upon the spectral induced polarization (SIP) response of clayey sands. The low-frequency quadrature conductivity of clay-sand mixtures may be related to the clay content, but also to the different types of clays constituting the samples. It depends on their specific surface area and surface charge density or alternatively to their CEC (Leroy and Revil, 2009; Weller and Slater, 2012; Revil, 2013).

The influence of the pore water chemical composition on induced polarization of clayey media was investigated, for instance, by Vacquier et al. (1957), Fraser et al. (1964), Klein and Sill (1982), Vinegar and Waxman (1984), and Revil et al. (2013a, 2013b). They show that the chargeability (a ratio of polarization to conduction) decreases when the salinity increases because conduction currents of the bulk pore water increase with salinity. In the frequency domain, Vinegar and Waxman (1984) also emphasize that the quadrature conductivity (polarization) of shaly sandstones depends slightly on salinity (NaCl) and increases with their CEC. Nevertheless, Vinegar and Waxman (1984) find that the quadrature conductivities of "clean" sands and weakly consolidated sandstones (with a low clay content $\leq 10\%$ of the sample mass) increase with NaCl concentration (from 0.5 to 2.0 $\mathrm{mol\,L^{-1}}$). Revil et al. (2013a, 2013b) observe that the quadrature conductivities of their saprolites samples (with 50% sand, 30% silt, and 20 wt% of illite and interstratified illite-smectite) increase with salinity (NaCl; from 0.003 to 0.3 $\mathrm{mol\,L^{-1}}$, $\mathrm{pH} = 5.7$).

With the exception of the recent works by Revil (2012) and Revil et al. (2013a, 2013b), previously published data have not been analyzed yet in terms of a mechanistic model of induced polarization. The reason for the lack of mechanistic model is probably related to the existence of several polarization mechanisms (membrane polarization, Stern layer polarization, and Maxwell-Wagner polarization; see Sen et al., 1984; Knight and Endres, 1990; Leroy et al., 2008; Leroy and Revil, 2009; Cosenza et al., 2009; Revil, 2012; Revil et al., 2013a, 2013b) that may explain the polarization spectra of clay materials. These polarization mechanisms may overlap in frequency (particularly in the kilohertz to megahertz range; Leroy and Revil, 2009; Revil, 2013).

Recently, Revil (2012) and Revil et al. (2013a, 2013b) show that the in-phase conductivity (conduction) of clay-sand mixtures is strongly related to the quadrature conductivity of the clayey materials. Conduction (electromigration) currents in the electric double layer (EDL) and in the bulk pore water are responsible for the in-phase conductivity response (Revil and Glover, 1997). Leroy and Revil (2004) report that surface conductivity of smectite appears rather independent of salinity, whereas for kaolinite, as for metal-oxide minerals, surface conductivity is known to increase with salinity (Leroy and Revil, 2004; Leroy et al., 2011; Leroy et al., 2013). A similar behavior may be expected for the quadrature conductivity because of the close relationship between surface and quadrature conductivities (Revil et al., 2013a, 2013b; Weller et al., 2013).

Leroy et al. (2008) and Leroy and Revil (2009) assume that the quadrature conductivity of saturated sands and clays is controlled by the electrochemical polarization of their Stern layer because the diffuse layer may be continuous at the scale of the porous continuum. The counterions in the Stern layer may move tangentially to the particle surface in response to the applied alternating electric field. This implies that the size, shape, surface roughness of the particles and surface site density, and mobility of the counterions in the Stern layer may influence the low-frequency quadrature conductivity of charged porous media. For well-sorted grains, the low-frequency quadrature conductivity depends on frequency because the discontinuity of the Stern layer between grains is responsible for the existence of polarization length scales controlled by the particle or pore size distribution (Lesmes and Morgan, 2001; Leroy et al., 2008; Revil and Florsch, 2010; Bücker and Hördt, 2013). The shape of the charged particles also influences their low-frequency quadrature conductivity. As shown by Grosse et al. (1999), Leroy and Revil (2009), and Jimenez and Bellini (2010), the magnitude of polarization currents around a highly charged particle (like a clay particle) increases with its aspect ratio. In addition, Leroy et al. (2008) show that the surface roughness of glass beads increases the broadness of the quadrature conductivity spectra. These authors also emphasize that the magnitude of the quadrature conductivity increases with the number of surface sites occupied by the counterions in the Stern layer.

Revil (2012) and Revil et al. (2013a, 2013b) argue that only mobile ions in the diffuse layer of clays (and not in the Stern layer) are responsible for conduction currents occurring at the surface of the particles. They state that the mobility of sodium counterions in the Stern layer of clays is very low (approximately 1/350th of their mobility in the bulk pore water) because of the high ion density populating the Stern layer. However, recent molecular dynamics (MD) simulations of the smectite-water interface with no applied electric field (Tournassat et al., 2009; Bourg and Sposito, 2011) argue that the diffusivity and therefore the resulting mobility of counterions in the Stern layer of clays is relatively high (for sodium ions, they found that their diffusivity in the Stern layer of smectite is approximately 0.5 times the value of their diffusivity in the bulk pore water). Therefore, the debate over the value of the mobility of counterions in the Stern layer of clays is still open and a complete data set of low-frequency complex conductivity measurements is still necessary to describe more accurately the conduction and polarization of clayey materials.

Downloaded 11/18/14 to 138.67.11.98. Redistribution subject to SEG license or copyright; see Terms of Use at http://library.seg.org/

To understand the effect of clay content and mineralogy and the effect of the pore water chemical composition on induced polarization of clayey media, we performed a new set of well-controlled laboratory induced polarization experiments with water-saturated unconsolidated clays and clay-sand mixtures. Our measurements are described by a new mechanistic induced polarization model, which considers electrochemical conduction of the Stern and diffuse layers around the particles with different sizes, electrochemical polarization of the Stern layer, and clay-sand mixtures. Our induced polarization model uses a Donnan equilibrium model to describe the electrochemical properties of the mineral-water interface. It also uses the full differential effective medium (DEM) theory (without any approximation regarding the shape of the particles or the ratio of the surface to bulk electric conductivity) to upscale particle conduction and polarization models to the (effective) complex conductivity model of the porous medium at the scale of its representative elementary volume.

MATERIAL AND METHODS

Samples preparation and analysis

Various clay-sand mixtures were prepared by mixing some Fontainebleau sand (a 99.98% silica-pure sand), clays, and an NaCl electrolyte at various salinities. We use clays containing mostly kaolinite and smectite. Chlorite has properties very similar to kaolinite, and illite has some properties that are intermediate between kaolinite and smectite (e.g., Leroy and Revil, 2004, 2009; Revil and Leroy, 2004;), so these two clay minerals were not considered in the present study. X-ray diffraction (XRD) analysis was used to determine the mineralogical content of the clays and sand samples before preparing our mixtures. The CEC of the clays was measured using the method proposed by Jackson (1964) (ammonium acetate adsorption), and their external specific surface areas S_s were measured using the Brunauer-Emmett-Teller (BET) method (nitrogen adsorption). The BET method does not provide the total specific surface area of smectites because it only probes the whole external surface of the clay particles and not the interlayer pore space (Tournassat et al., 2013). A summary of these experimental results is given in Table 1. These preliminary analyses allowed classifying clay samples in two classes, K1 and K2 for kaolinite, due to their slightly different mineralogical contents, and B1 and B2 for bentonite (Portaclay A90; Ankerpoort, Maastricht, The Netherlands). K1 clay is characterized by a nonnegligible fraction of smectite (15 wt%). Therefore, this sample is not a pure kaolinite sample. The CEC of B2 (0.442 $\mathrm{meq\,g^{-1}}$) is higher than that for B1 (0.34 $\mathrm{meq\,g^{-1}}$). Particle size measurements were performed in vacuum using a laser granulometer (the data will be discussed below in the paper). The measurements of the bulk pore water electric conductivity were made with a Multi 340i-WTW conductimeter before mixing the electrolytes to the solid phase (the values will be shown later in the paper).

Mixtures were prepared by varying the volumetric clay fractions, the clay mineralogy (K1, K2, B1, and B2), and the salinity (distilled water, 0.1 $\mathrm{g\,L^{-1}}$, 1 $\mathrm{g\,L^{-1}}$, and 10 $\mathrm{g\,L^{-1}}$ NaCl), to study the impact of these factors upon the low-frequency induced polarization spectra. We first prepared the 100% clay end member by adding the saturating fluid (degassed distilled water) to the clays. Then, the volumetric clay fraction was reduced to 20%, 5%, and 1% (depending on the sample) by adding sand grains to the mixture. The preparation of mixtures was performed by combining first the solid phases (clay-sand) until a homogeneous distribution is achieved (in a blender) and then the degassed saturating fluid is added under vacuum. This procedure was repeated for different types of clays and different salinities. The gravimetric water content and the porosity ϕ of each mixture (Table 2) were measured by weighting dry and wet samples taken from each mixture after each SIP measurement.

Experimental setup

Frequency-domain induced polarization measurements consist of imposing a harmonic current I (in A) at a given frequency and measuring the resulting electric potentials' difference U (in volts) between two nonpolarizing voltage electrodes. The impedance, $Z^*(\omega)$ (in ohm, Ω), is

$$Z^*(\omega) = \frac{U}{I} = |Z^*(\omega)|e^{i\varphi(\omega)}, \tag{1}$$

where φ is the phase angle (in rad) and ω is the angular frequency (in rad $\mathrm{s^{-1}}$; $\omega = 2\pi f$ with f being the frequency in hertz or $\mathrm{s^{-1}}$). The complex resistivity $\rho^*(\omega)$ (in Ω m) is related to $Z^*(\omega)$ by a geometric factor K (in meters) ($\rho^*(\omega) = KZ^*(\omega)$). This geometric factor takes into account not only the position of the electrodes, but also the size and shape of the samples, and the boundary conditions on their surface. The geometric factor value of 0.45 m was computed by solving numerically the Poisson equation using COMSOL Multiphysics software (version 3.5a). This value was confirmed by an experimental measurement with the SIP FUCHS II device, which was carried out with the sample holder of interest (Figure 1) filled with a conductive electrolyte (with known electric conductivity).

The complex electric conductivity $\sigma^*(\omega)$ (in $\mathrm{S\,m^{-1}}$) is written as

$$\sigma^*(\omega) = \frac{1}{\rho^*(\omega)} = \sigma'(\omega) + i\sigma''(\omega), \tag{2}$$

$$\varphi(\omega) = \tan^{-1}\left[\frac{\sigma''(\omega)}{\sigma'(\omega)}\right] \cong \frac{\sigma''(\omega)}{\sigma'(\omega)}. \tag{3}$$

Table 1. Measured mineralogical composition (in weight percent), CEC and external specific surface areas S_s of the samples used to prepare clay-sand mixtures. Kaolinite (K) clays and bentonite (B) clays are divided in two classes because of their slightly different mineralogical compositions. S stands for sand. The error concerning the quantitative determination of mineral phases with the XRD method is about ±5% (clay fraction < 2 μm; see Holtzapffel, 1985).

Minerals	K1	K2	B1	B2	S
Kaolinite	0.80	0.95	0.05	0.05	0
Illite-muscovite	0.05	0.05	0.00	0.00	0
Smectite	0.15	0	0.95[9]	0.95[10]	0
Silica	0	0	0	0	0.9998
CEC ($\mathrm{meq\,g^{-1}}$)	<0.10	<0.10	0.34	0.442	—
External S_s ($\mathrm{m^2\,g^{-1}}$)	9.4	12.6	30	27	0.5

[9] Na-montmorillonite.

[10] Ca-Na-montmorillonite.

Downloaded 11/18/14 to 138.67.11.98. Redistribution subject to SEG license or copyright; see Terms of Use at http://library.seg.org/

The last approximation in the second part of equation 3 holds for a phase magnitude smaller than 100 mrad. In equations 1 and 2, $i = \sqrt{-1}$ represents the pure imaginary number. The phase angle $\varphi(\omega)$ defines the ratio of the polarization to the electromigration (conduction) currents. To separate the electromigration and polarization effects, it is more instructive to plot the in-phase and quadrature components of the complex conductivity rather than the magnitude of the conductivity and the phase lag (Vinegar and Waxman, 1984).

The sample holder used in our investigations consists of a cylinder made of polyvinyl chloride with a 30-cm length and a 20-cm diameter. The nonpolarizing ($Cu\text{-}CuSO_4$) electrodes were installed 5 cm from the base of the sample holder and are regularly spaced (each 90°; see Figure 1). The $Cu\text{-}CuSO_4$ electrodes (6-mm diameter with porous ceramics at their ends) were used to inject the current and to measure the potential difference. The first set of four electrode measurements was carried out immediately after the preparation of the mixtures using the commercial SIP FUCHS II impedance meter from Radic Research. The SIP FUCHS II measures the complex conductivity over $P = 7$ decades in frequency (1.4 mHz–12 kHz). For a resistor-capacitor network, the error on the phase lag (the instrument accuracy) is about ±1 mrad on the measurements for frequencies greater than 6 kHz. For lower frequencies, the accuracy on the phase lag is better than ±0.5 mrad (Weller and Börner, 1996; Binley et al., 2005). We also used the PSM1735 NumetriQ impedance meter to compare both

Table 2. Overview of the prepared mixtures with different clay samples. The * symbol indicates that the sensitivity of the impedance meter was too low to achieve the spectral induced polarization measurements. The — symbol indicates that the clay samples were out of stock. Porosity is given in pore volume fraction.

		Salinity of saturating fluid			
Volumetric clay fraction in the mixture	Porosity	Distilled water	0.1 $g\,L^{-1}$	1 $g\,L^{-1}$	10 $g\,L^{-1}$
K1 mixtures					
100	0.55	√	√	√	√
20	0.30	√	√	√	√
5	0.30	√	—	—	—
1	0.35	√	√	√	√
K2 mixtures					
100	0.57	√	√	√	*
20	0.31	√	√	√	*
5	0.31	√	√	√	*
1	0.35	√	√	√	*
B1 mixtures					
100	0.83	√	√	—	—
20	0.51	√	—	—	—
5	0.46	√	—	—	—
1	0.43	√	—	—	—
B2 mixtures					
100	0.84	√	√	*	*
20	0.50	√	√	√	√
5	0.38	√	√	√	√
1	0.49	√	√	√	√

Downloaded 11/18/14 to 138.67.11.98. Redistribution subject to SEG license or copyright; see Terms of Use at http://library.seg.org/

instruments. The instrumental error on the phase lag is about $\pm 0.87\,\mathrm{mrad}$ for frequencies smaller than $35\,\mathrm{mHz} + 0.0017\,\mathrm{mrad/kHz}$.

We performed two types of tests to control the quality and reproducibility of the SIP response. A first set of tests was carried out with both devices using the pure resistances of (5, 15, and 30 Ω) for SIP Fuchs II and (10, 15, and 30 Ω) for PSM1735-NumetriQ (Figure 2). In the case of the lower resistance of 5 Ω, the SIP Fuchs II gives a very small maximum error of 0.5 mrad for frequencies smaller than 1 kHz. Therefore, for the lowest resistivity values of the clay-sand mixtures (approximately 2 Ω m, therefore a resistance of ~4 Ω), we consider that the maximum experimental error is roughly 0.5 mrad for frequencies smaller than 1 kHz. In the second series of tests, we performed SIP measurements with the same clay-sand mixtures using both impedance meters to compare their responses. The obtained phase spectra are in excellent agreement with each other except for a slight difference at frequencies higher than 1 kHz (see Figure 3). These tests allow us to consider that the two devices give comparable results. The reason for homogeneous current field is not needed for our high-quality spectra. It is usually required for a heterogeneous sample to get a representative volume of the rock. In our case, the samples are homogeneous much lower than the size of the sample holder and therefore our procedure is perfectly adequate.

For all of the measurements, the same protocol was followed. Before starting the measurements, frequency-domain induced polarization measurements were performed using pure resistances of 100 and 221 Ω and the two impedance meters (to calibrate them). The measurements with the clay-sand mixtures were repeated one to five times during the same day and again over a period of two to five days to improve the signal-to-noise ratio. At the end of each day, the nonpolarizing electrodes were removed from the sample holder to prevent a possible diffusion of their filling solution into the clay-sand mixtures. The sample holder was maintained hermetically packed during and after the measurements to minimize its desaturation. During all of the experiments, the relative humidity and temperature were in the range of 48 ± 18% and 23.8 ± 3°C, respectively.

THEORY

Induced polarization model

An SIP model based on the Schurr model (Schurr, 1964) is developed below. The Schurr model unified the O'Konski theory (O'Konski, 1960) for the description of conduction current densities and the Schwarz theory (Schwarz, 1962) for the description of polarization current densities at the surface of the particle. Lesmes and Morgan (2001) and Revil and coworkers (Leroy et al., 2008; Leroy and Revil, 2009; Jougnot et al., 2010; Revil and Florsch, 2010) successfully use the Schurr model for the prediction of the complex conductivity spectra of various materials (glass beads, quartz, clays) and rocks (sandstones, Berea, and shaly sandstones) in water-saturated and unsaturated conditions. Their SIP model and ours include the electrochemical polarization of the Stern layer as well as the Maxwell-Wagner polarization. They also include the effect of the particle size distribution (PSD) (this is very useful when the quadrature conductivity appears frequency dependent) and assume (except the work of Lesmes and Morgan, 2001) that the diffuse layer is continuous at the scale of the porous medium (Figure 4). Nevertheless, their SIP model and ours do not consider the back-diffusion of salt ions through different pore spaces of the material (cation-selective zones and zones with no selectivity), which is responsible for a polarization process named *membrane polarization* (Marshall and Madden, 1959; Vinegar and Waxman 1984). Membrane polarization is a complex phenomenon, which is difficult to account at this stage in our model (see Bücker and Hördt, 2013 for an attempt to model this contribution).

Revil (2012) and Revil et al. (2013a, 2013b) develop several mechanistic SIP models for clay-sand mixtures. These models are also based on the electrochemical polarization of the Stern layer coating the particles, but they used the surface conductivity model of Kan and Sen (1987). This electric conductivity model relies directly on the in-phase component of the surface conductivity to the total porosity, apparent surface mobility of counterions in the EDL, and the volumetric excess of the charge per unit pore volume of the material (Revil, 2012). The electrochemical conduction and polarization model of Schurr (1964) has the advantage of being able to directly link to the surface electrochemical properties (ion mobilities, surface site densities) of the electric double layer (Stern and diffuse layer). The SIP model of Leroy and Revil (2009) and ours are based on the Schurr (1964) model (for grain conduction and polarization) and on the DEM theory (used to upscale the complex

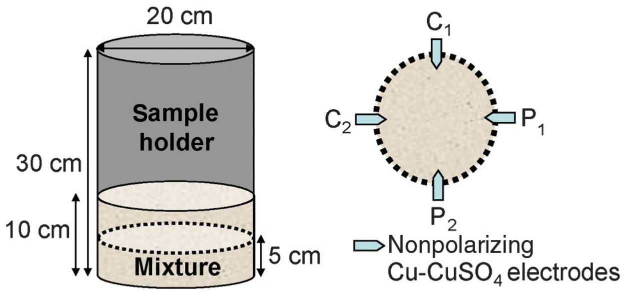

Figure 1. Sketch of the sample holder showing the position of the four electrodes for the SIP measurement.

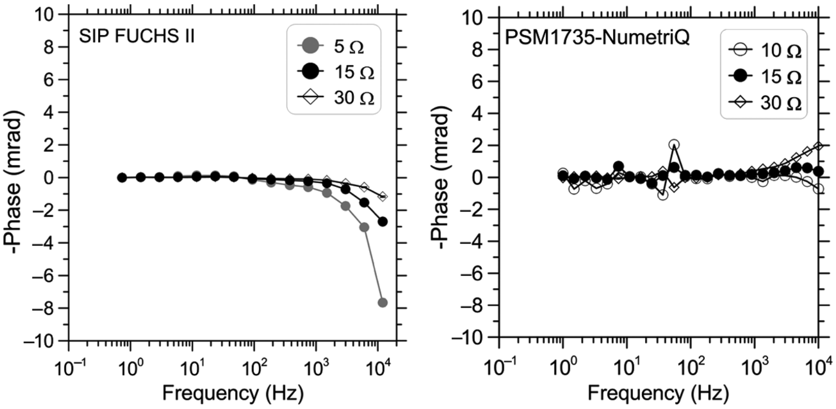

Figure 2. Phase spectra measured with SIP FUCHS II (left; resistors of $R = 5$ Ω, 15, and 30 Ω) and measured with the PSM1735 NumetriQ (right; resistors of $R = 10$, 15, and 30 Ω). Errors were calculated by the measurement devices and are not significant.

Downloaded 11/18/14 to 138.67.11.98. Redistribution subject to SEG license or copyright; see Terms of Use at http://library.seg.org/

surface conductivity model at the scale of the sample). The differences are as follows:

1) Our calculation of the surface site densities of adsorbed ions in the Stern and diffuse layers is based on the Donnan equilibrium model (Revil and Leroy, 2004; Leroy et al., 2007). Leroy and Revil (2009) use a triple-layer model (TLM) to validate their fitted surface site densities of adsorbed ions according to complex impedance measurements of clay gels. However, the TLM alone is not adapted for describing the electrochemical properties of clay-rich porous media because it was developed for perfectly flat, homogeneous, and noninteracting metal electrodes (Hunter, 1981), whereas the Donnan equilibrium model can be used for rough particles with interacting diffuse layers (Tournassat and Appelo, 2011).

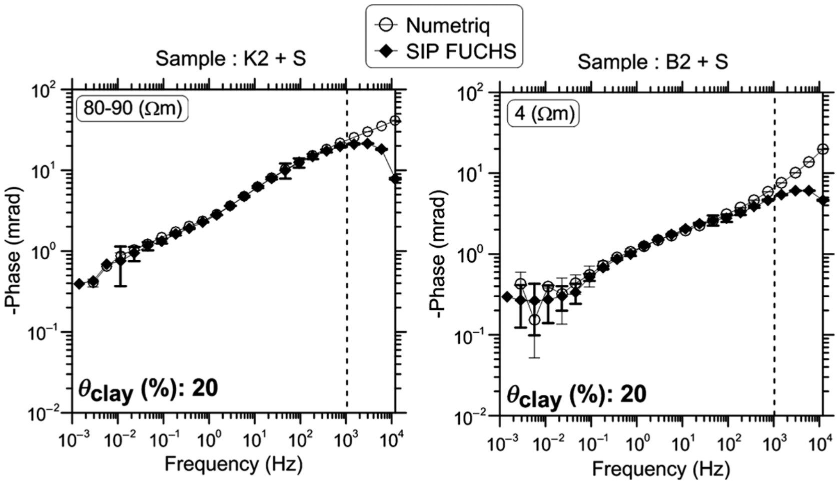

Figure 3. Comparison of the phase response of two measuring impedance meters through clay-sand mixtures prepared with Fontainebleau sand (S), kaolinite ("K2"), and bentonite ("B2") clay with 20% clay content (in volume). Mixtures are saturated with distilled water. The mean resistivity amplitude of the K2 + S mixtures is on the order of 80–90 Ωm and 4 Ωm for the B2 + S mixtures. The error bars correspond to twice the standard deviation computed on three cycles at each frequency.

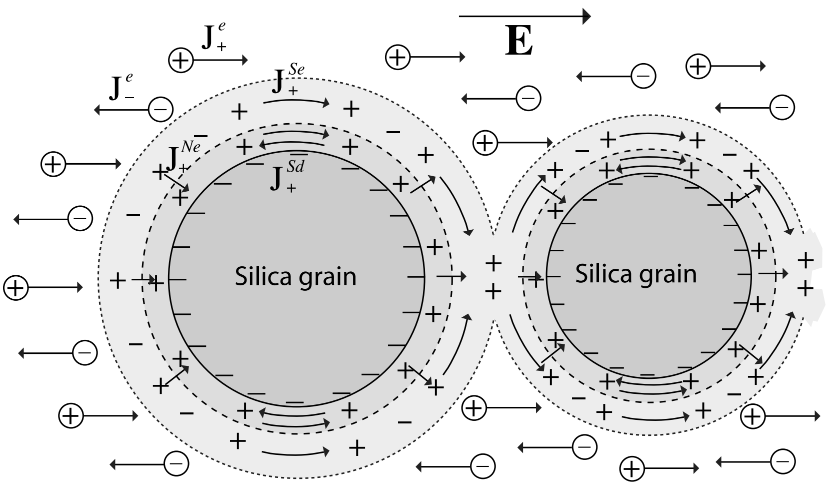

Figure 4. Sketch of the revisited electrochemical conduction and polarization model of Leroy et al. (2008) for silica particles immersed in 1:1 aqueous electrolyte (for instance, NaCl or KCl). The presence of an alternating applied electric field **E** is responsible for conduction and polarization current densities in the electric double layer around negatively charged grains. Our electric double layer is composed of a Stern layer (containing only counterions and located very close to the surface) and of a diffuse layer (containing mostly counterions). Mobile ions electromigrate under the influence of the electric field and are responsible for conduction current densities parallel to the electric field direction $\mathbf{J}^{e}_{\pm}$, normal $\mathbf{J}^{Ne}_{\pm}$ and parallel to the grain surface $\mathbf{J}^{Se}_{\pm}$ (current densities of coions are not represented to clarify the picture). Ions in the Stern layer diffuse back at the surface of the grain, and are responsible for diffusion current densities $\mathbf{J}^{Sd}_{+}$ and a resulting polarization of the Stern layer. Ions in the diffuse layer do not polarize it because the diffuse layer forms a continuous medium at the scale of the porous medium. The discontinuity of the Stern layer is responsible for polarization currents densities depending on the PSD.

2) The new induced polarization model considers the contribution of the Stern layer to the DC surface conductivity. Leroy et al. (2008) and Leroy and Revil (2009) assume that the Stern layer polarizes but does not participate to electromigration currents, therefore, that the contribution of the Stern layer to the DC surface conductivity was equal to zero (this is exactly the result of the Schwarz, 1962 theory). This may be not correct, especially for quartz sands, because sodium counterions adsorbed in their Stern layer, as outer sphere complexes, are known to be relatively mobile (compared to their mobility in bulk pore water; see Leroy et al., 2013). Conduction and polarization currents may occur simultaneously in the Stern layer, which acts as a leaking capacitance. This assumption is justified by the low magnitude of the applied alternating electric field during complex impedance measurements. It may not change significantly the initial concentration of counterions in the Stern layer (at thermodynamic equilibrium; see Figure 4). Therefore, a resulting very small variation of the concentration of counterions in the Stern layer may induce electromigration currents that are independent of polarization currents (Schurr, 1964). Lesmes and Morgan (2001) also use this assumption for the Berea sandstones.
3) Our modeling of the conduction and polarization currents is not restricted to monovalent cations in the Stern layer. However, only polarization currents due to the surface diffusivity of one type of counterions (for instance, Na^+ or Ca^{2+}) can be modeled by our induced polarization model (our complex conductivity model cannot predict the polarization of the Stern layer constituted of different types of ions such as Na^+ and Ca^{2+}, for instance).
4) Our complex surface conductivity model considers mixtures of clays and sand, which is not the case of the SIP model of Leroy and Revil (2009).
5) Another difference between the two SIP models is the upscaling approach. Leroy and Revil (2009) use an analytical solution of

Downloaded 11/18/14 to 138.67.11.98. Redistribution subject to SEG license or copyright; see Terms of Use at http://library.seg.org/

the DEM theory (Bruggeman, 1935; Hanai, 1968; Sen et al., 1981; Mendelson and Cohen, 1982), which is useful for low Dukhin numbers (the Dukhin number depends on the ratio of the surface to bulk electric conductivity; Dukhin and Shilov, 1974). This was justified by the highly conductive pore water of clays relative to their surface conductivity. The DEM equations of the new induced polarization model are solved numerically without any assumption regarding the Dukhin number or the shape of the particles.

Donnan equilibrium model

The electric potential in the diffuse layer, ψ_m (in volts) and the resulting surface site densities of adsorbed ions in the diffuse and Stern layers Γ_i^d and Γ_i^{St} (in sites m^{-2}) are calculated using the Donnan equilibrium model (Donnan, 1924) and the approach developed by Revil and Leroy (2004) and Leroy et al. (2007). The value of ψ_m is calculated numerically by solving the following equation (the ionic concentrations in the bulk pore water C_i^f are supposedly known; Leroy et al., 2007):

$$e1000N_A\sum_{i=1}^{N}\pm z_iC_i^f\exp\left(-\frac{\pm ez_i\psi_m}{k_bT}\right) - (1-f_Q)Q_V = 0, \tag{4}$$

where e is the electronic charge (1.602×10^{-19}C), N_A is the Avogadro number (6.022×10^{23} mol^{-1}), N is the number of types of ions in the aqueous electrolyte, "+" stands for cations and "−" stands for anions, z_i is the ion valency, k_b is the Boltzmann constant (1.381×10^{-23} $\mathrm{J\,K}^{-1}$), T is the temperature (in degree kelvin). The parameters of equation 4 are f_Q, which is the partition coefficient, and Q_V, which is the excess of charge per unit pore volume of the material (in $\mathrm{C\,m}^{-3}$).

The partition coefficient describes the fraction of the charge located in the Stern layer with respect to the total charge contained in the Stern and diffuse layers (that counterbalances the charge on the mineral surface). It can be calculated by a TLM (Leroy et al., 2008) when diffuse layers don't interact each other, which is rarely the case in reality. The partition coefficient is defined by

$$f_Q \equiv \frac{Q_{St}}{Q_{St}+Q_d} = \frac{\sum_{i=1}^{M}\pm z_i\Gamma_i^{St}}{\sum_{i=1}^{M}\pm z_i\Gamma_i^{St}+\sum_{i=1}^{N}\pm z_i\Gamma_i^{d}}, \tag{5}$$

where M is the number of types of adsorbed ions in the Stern layer, Γ_i^{St} and Γ_i^d are the surface site densities (in sites m^{-2}), and Q_{St} and Q_d are the surface charge densities of the Stern and diffuse layers (in $\mathrm{C\,m}^{-2}$), respectively. If only one type of counterion is present in the Stern layer, equation 5 reduces to

$$f_Q = \frac{z_i\Gamma_i^{St}}{z_i\Gamma_i^{St}+\sum_{i=1}^{N}\pm z_i\Gamma_i^{d}}. \tag{6}$$

The excess of charge per unit pore volume of sands can be calculated as a function of their specific surface area S_S (in $\mathrm{m}^2\,\mathrm{g}^{-1}$) multiplied by their surface charge density Q_0 (in $\mathrm{C\,m}^{-2}$), whereas the excess of charge per unit pore volume of clays can be calculated directly as a function of their CEC (in meq g^{-1}). The value of Q_V is determined by using the following equations (Waxman and Smits, 1968):

$$Q_V = -\rho_g\left(\frac{1-\phi}{\phi}\right)10^3 S_s Q_0, \tag{7}$$

$$Q_V = \rho_g\left(\frac{1-\phi}{\phi}\right)eN_A\mathrm{CEC}, \tag{8}$$

$$\mathrm{CEC} = -\frac{10^3 S_s}{eN_A}Q_0, \tag{9}$$

where ρ_g is the volumetric grain density (in $\mathrm{kg\,m}^{-3}$). At the opposite of ρ_g, ϕ, and S_s, the surface charge density of sands depends on the chemical composition of the bulk pore water. Deprotonation of hydroxyl surface sites of sands and ions adsorption in the electric double layer are responsible for the increase of the magnitude of Q_0 with pH and salinity (Sahai and Sverjensky, 1997; Leroy et al., 2013). The excess of charge per unit pore volume of sands may therefore increase with pH and salinity because of the increase of the magnitude of the surface charge density. Because of isomorphic substitutions in the crystal lattice of clays, surface charge densities of the basal planes of smectites and illites (and in a lesser extent of kaolinites) can be considered constant with pH and salinity (Tombacz and Szekeres, 2004, 2006; Leroy et al., 2007; Tournassat and Appelo, 2011). The excess of charge per unit pore volume of these clays may therefore be assumed constant with salinity because of the constant surface charge density. Therefore, it can be expressed as a function of the CEC (Revil et al., 1998). Nevertheless, in the Donnan equilibrium model, the porosity parameter entering in equations 7 and 8 is in reality the fraction of the pore volume occupied by the double layer. But, it is very hard to estimate the pore volume occupied by the double layer, and, for that reason, the porosity is used in equations 7 and 8.

The surface site density of ions in the diffuse layer Γ_i^d (in sites m^{-2}) can be calculated as a function of C_i^f and ψ_m:

$$\Gamma_i^d = 1000N_A\Delta C_i^f\left[\exp\left(-\frac{\pm ez_i\psi_m}{k_bT}\right)-1\right], \tag{10}$$

where Δ (in meters) is the half-thickness of the mean pore size. When the EDL occupies the whole pore space, and when there are no interacting diffuse layers, $\Delta\approx 2\chi_d$, where χ_d is the Debye length (in meters; Hunter, 1981; Tournassat and Appelo, 2011). The Debye length (in meters) is calculated by

$$\chi_d \equiv \sqrt{\frac{\varepsilon_f k_b T}{e^2 2000 N_A I}}, \tag{11}$$

where ε_f is the dielectric permittivity of the diffuse layer (in $\mathrm{F\,m}^{-1}$) ($\varepsilon_f\equiv\varepsilon_r\varepsilon_0$, where ε_r is the relative dielectric permittivity of water, 78.3 at a temperature of 298 K and pressure of 1 bar; ε_0 is the dielectric permittivity of vacuum, 8.85419×10^{-12} $\mathrm{F\,m}^{-1}$); and I is the ionic strength of the bulk pore water (in $\mathrm{mol\,L}^{-1}$), which is defined by

Downloaded 11/18/14 to 138.67.11.98. Redistribution subject to SEG license or copyright; see Terms of Use at http://library.seg.org/

$$I \equiv \frac{1}{2}\sum_{i=1}^{N} z_i^2 C_i^f. \tag{12}$$

By combining equations 6 and 10, the surface site density of the adsorbed ions in the Stern layer Γ_i^{St} can be calculated as a function of f_Q, C_i^f, and ψ_m:

$$\Gamma_i^{St} = \frac{1000 N_A \Delta}{z_i}\left(\frac{f_Q}{1-f_Q}\right)\sum_{i=1}^{N} \pm z_i C_i^f \left[\exp\left(-\frac{\pm e z_i \psi_m}{k_b T}\right)-1\right]. \tag{13}$$

In summary, we have developed a Donnan equilibrium model to estimate the surface site densities of adsorbed ions in the Stern and diffuse layers Γ_i^{St} and Γ_i^{d} which are responsible for conduction and polarization current densities at the surface of the particles. These parameters depend on the chemical composition of bulk pore water, on the partition coefficient f_Q and on the excess of charge per unit pore volume Q_V. Q_V depends on intrinsic petrophysical properties of the sample (grain density, porosity, and specific surface area), but also on its surface charge density. The magnitude of the surface charge density of sands increases with pH and salinity, whereas the surface charge density of smectites and illites (and to a lesser extent of kaolinites) can be assumed constant with pH and salinity. Therefore, the CEC of these clays can be directly used to estimate their excess of charge per unit pore volume. The methodology used for the calculation of the surface sites densities of adsorbed ions in the Stern and diffuse layer is presented in Figure 5.

Complex surface conductivity model

Conduction and polarization currents at the surface of the charged particle are modeled using the modified complex surface conductivity model of Leroy et al. (2008). These authors assume that ions in the Stern layer can only participate to polarization currents. However, contrary to the complex surface conductivity model of Leroy et al. (2008), because of the low magnitude of the applied electric field during SIP experiments, in our approach, ions in the Stern layer can participate to conduction and polarization currents. The complex surface conductivity of a charged spherical grain of diameter d_0 immersed in an aqueous electrolyte is described using the following equations:

$$\sigma_S^*(d_0,\omega) = \frac{4}{d_0}\left(\Sigma_S^{St}+\Sigma_S^0\right) - \frac{4}{d_0}\frac{\Sigma_S^{St}}{1+i\omega\tau_0} + i\omega\varepsilon_g, \tag{14}$$

$$\Sigma_S^{St} = e z_i \beta_i^{St} \Gamma_i^{St}, \tag{15}$$

$$\Sigma_S^0 = \Sigma_S^{St} + \Sigma_S^d = e z_i \beta_i^{St} \Gamma_i^{St} + \sum_{i=1}^{N} e z_i \beta_i^d \Gamma_i^d, \tag{16}$$

$$\tau_0 \equiv \frac{1}{f_0} = \frac{e z_i}{8 k_b T}\frac{d_0^2}{\beta_i^{St}}, \tag{17}$$

$$\varepsilon_g = 0.00191 \rho_g \varepsilon_0, \tag{18}$$

where σ_S and ε_g are the surface electrical conductivity and internal dielectric permittivity of the particles, respectively. The specific surface conductivity Σ_S^{St} (in siemens) represents the frequency-dependent (alternating current) contribution (electrochemical polarization) of the Stern layer to the complex surface conductivity (Leroy et al., 2008). Σ_S^0 is the frequency-independent (DC) contribution (electromigration) of the Stern Σ_S^{St} and of the diffuse layer Σ_S^d to the complex surface conductivity (Revil and Glover, 1997). The value of Σ_S^0 is calculated using the O'Konski theory (O'Konski, 1960). In equation 18, the surface dielectric permittivity of the particles is esti-

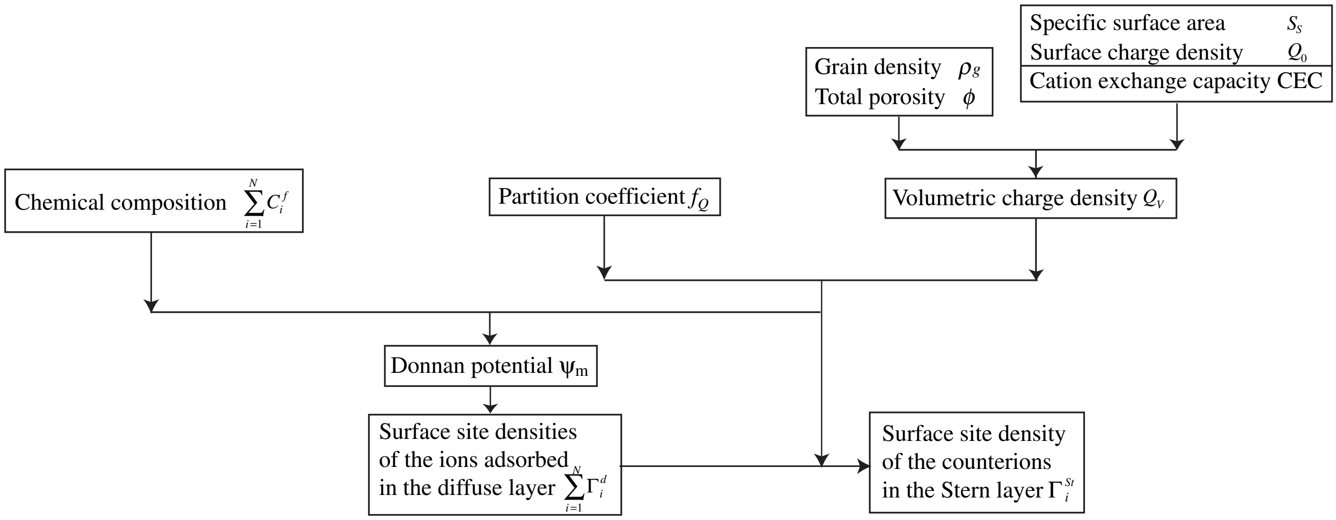

Figure 5. Modeling strategy for determining the surface site densities of adsorbed ions in the Stern and diffuse layers at a given chemical composition of the bulk aqueous electrolyte. The main parameters of the Donnan equilibrium model are the partition coefficient between the surface charge densities of the Stern and diffuse layer f_Q and the volumetric charge density of the pore water Q_V. The value of Q_V is calculated using the grain mass density ρ_g, total porosity ϕ, and the specific surface area S_s, surface charge density Q_0 (sands) or the CEC (clays).

Downloaded 11/18/14 to 138.67.11.98. Redistribution subject to SEG license or copyright; see Terms of Use at http://library.seg.org/

mated as a function of the grain density ρ_g because of the absence of lossy materials (magnetic or metallic minerals, Fe Ti sulfides oxides such as ilmenite; Olhoeft, 1981). In equations 15–17, β_i^{St} and β_i^d are the ion mobility (in $\mathrm{m^2\,s^{-1}\,V^{-1}}$) in the Stern and diffuse layer, respectively. The parameters β_i^{St} and β_i^d (to a lesser extent) remain relatively unknown because of the effects of ions and mineral surface on the ion mobilities in the Stern and diffuse layers. Because the diffuse layer is far (several angstroms) from the mineral surface, we assume that the ion mobility in the diffuse layer is equal to the ion mobility in the bulk pore water, i.e., $\beta_i^d \approx \beta_i^f$. The value of β_i^f can be calculated using the Nernst-Einstein equation and measured ionic diffusivities in dilute aqueous solutions (Revil, 1999; Revil and Leroy, 2004). The symbol τ_0 is the relaxation time (in seconds), and f_0 is the characteristic frequency (in Hz).

We consider that the diffuse layer of the kaolinite-sand mixtures does not fill a large fraction of the pore volume because of the very small specific surface areas of kaolinite and sand grains (compared to smectite grains; ~15 $\mathrm{m^2\,g^{-1}}$ for perfectly dispersed kaolinites particles; see, e.g., Revil and Leroy, 2004). Bentonites have very high specific surface areas (typically >500 $\mathrm{m^2\,g^{-1}}$) because they contain mostly smectites (Leroy et al., 2006). This implies that the diffuse layer of bentonites and bentonite-sand mixtures may occupy a large part of the connected porosity (Leroy and Revil, 2009; Tournassat and Appelo, 2011). For these reasons, we assume that the diffuse layer of bentonites participates to the electric conductivity of the pore space and not to the excess of electric conductivity at the surface of the particles; i.e., we assume that $\Sigma_S^d = 0$ S in equation 16 (Leroy and Revil, 2009). Following the arguments presented above, we assume that the pore water of kaolinite samples is occupied by the bulk water and that the pore water of bentonite samples is occupied by the diffuse layer.

As discussed by Revil (2012), a big unknown is however the value of the surface mobility of the counterions in the Stern layer of clays. Tournassat et al. (2009) and Bourg and Sposito (2011) compute MD simulations of the smectite-saline water interface (NaCl, and mixed NaCl and $\mathrm{CaCl_2}$ electrolytes, respectively). They found that the tangential diffusivity of sodium ions in the Stern layer of smectites is approximately half their diffusivity in the bulk pore water. More recently, Revil (2012) and Revil et al. (2013a, 2013b), in their SIP model, advocate for a mobility of the sodium ions in the Stern layer of clays that is two orders of magnitude smaller than their mobility in the bulk pore water. Therefore, MD simulations predict considerably higher mobility of sodium ions in the Stern layer of smectite compared to the mobility of sodium ions in the Stern layer of smectite given by the recent SIP models of Revil and coworkers.

The complex surface conductivity of the pure materials constituted of particles with different sizes is determined by averaging the net polarization of each particle over the entire distribution of particle sizes (Lesmes and Morgan, 2001). By assuming the superposition principle, i.e., that the surface conduction and polarization current densities of the particles all add in parallel, we obtain the following equation for the complex surface conductivity of the pure materials:

$$\sigma_S^* = \sum_{i=1}^{Q} f(d_{0i})\sigma_S^*(d_{0i}, \omega). \tag{19}$$

The parameter $f(d_{0i})$ is the discretized version of the PSD denoted by $f(d_0)$. The normalization of the PSD implies

$$\sum_{i=1}^{Q} f(d_{0i}) = 1, \tag{20}$$

which means that $f(d_{0i})$ is in fact a weight coefficient depending entirely on the PSD.

The SIP model developed here considers the conduction and polarization currents of the Stern layers around the particles with different sizes and that the diffuse layer only participates to conduction (electromigration) currents. The complex surface conductivity of pure clays and sand σ_S^* is calculated using the computed values of the surface sites densities of adsorbed ions in the Stern and diffuse layer Γ_i^d and Γ_i^{St} and the discretized PSD. The surface ion mobility in the Stern layer β_i^{St} is a key parameter of our induced polarization model because it governs the magnitude of the polarization currents (i.e., the magnitude of the quadrature conductivity) and the characteristic frequency associated with the electrochemical polarization of the Stern layer around the particles (i.e., the behavior of the quadrature conductivity as a function of the frequency). The parameter β_i^{St} may also influence the in-phase conductivity because we assume that the Stern layer can participate to conduction and polarization currents. In the following section, the DEM theory is used to upscale the complex surface conductivity model to the complex conductivity model of the sample.

Complex conductivity model of the sample

The porous medium of interest is divided into three main parts: the microporous clays, the sand grains, and the macropores between sand grains (Figure 6). The elongated clay particles coat the larger and spherical sand grains. Clays contain a diffuse layer (bentonites) or bulk pore water (kaolinites), and the Stern layer around clays and sand of different sizes controls the quadrature conductivity of the sample. Macropores contain bulk pore water.

The complex electric conductivity of the bulk pore water is calculated according to the following equation that considers conduction and displacement currents:

$$\sigma_f^* \equiv \sigma_f + i\omega\varepsilon_f, \tag{21}$$

where σ_f is the DC electric conductivity of the brine. During our SIP experiments, σ_f was measured using a conductimeter before the introduction of brine into clays. But, the electric conductivity of the bulk pore water can also be calculated using the known chemical composition in the limit of a dilute aqueous solution:

$$\sigma_f = e1000N_A \sum_{i=1}^{N} z_i \beta_i^f C_i^f, \tag{22}$$

where specific interactions between different types of ions are neglected. This assumption is valid for low to medium ionic strengths <1 $\mathrm{mol\,L^{-1}}$ (Revil, 1999).

The electric conductivity of the diffuse layer of bentonites is calculated using equations similar to equations 21 and 22, except that the ionic concentrations and mobilities in the bulk pore water and replaced by their associated ionic concentrations and mobilities in the diffuse layer (Revil and Glover, 1997). This implies, by using a Donnan ionic distribution in the pore water:

Downloaded 11/18/14 to 138.67.11.98. Redistribution subject to SEG license or copyright; see Terms of Use at http://library.seg.org/

$$\sigma_d^* = e1000N_A \sum_{i=1}^{N} z_i \beta_i^f C_i^f \exp\left(-\frac{\pm e z_i \psi_m}{k_b T}\right) + i\omega\varepsilon_f, \tag{23}$$

where we assume that the ionic mobilities and the water dielectric permittivity in the diffuse layer are equal to the ionic mobilities and the water dielectric permittivity in the bulk pore water, i.e., $\beta_i^d \approx \beta_i^f$ and $\varepsilon_d \approx \varepsilon_f$, respectively. It should be noted that equations 16, 22, and 23 don't consider the electro-osmotic water flow due to the applied electric field in the diffuse layer and bulk water because of the assumption of a low applied electric field.

The DEM theory (Bruggeman, 1935; Hanai, 1968; Sen et al., 1981; Mendelson and Cohen, 1982; Revil, 2000) is used for the calculation of the complex electric conductivity of the water saturated clays (i.e., of the clays particles and of their pore water). The initial electric conductivity of the water saturated clays is the electric conductivity of their pore water σ_w^* ($\sigma_w^* = \sigma_f^*$ in the case of kaolinite samples or $\sigma_w^* = \sigma_d^*$ in the case of bentonite samples). Inclusions are clay particles of surface conductivity σ_{Sc}^* (including the effect of the PSD on the surface conductivity) and volume fraction $d\Omega_{Sc}$. The value of σ_c^* is calculated iteratively using a MATLAB procedure and the following equations:

$$L = \frac{3 + \sqrt{9 + 36m^2 - 60m}}{6m}, \tag{24}$$

$$d\sigma_c^* = \frac{\sigma_c^*}{3} \frac{(\sigma_{Sc}^* - \sigma_c^*)[(1+3\,L)\sigma_{Sc}^* + (5-3\,L)\sigma_c^*]}{[L\sigma_{Sc}^* + (1-L)\sigma_c^*][(1-L)\sigma_{Sc}^* + (1+L)\sigma_c^*]} \frac{d\Omega_{Sc}}{1-\Omega_{Sc}}, \tag{25}$$

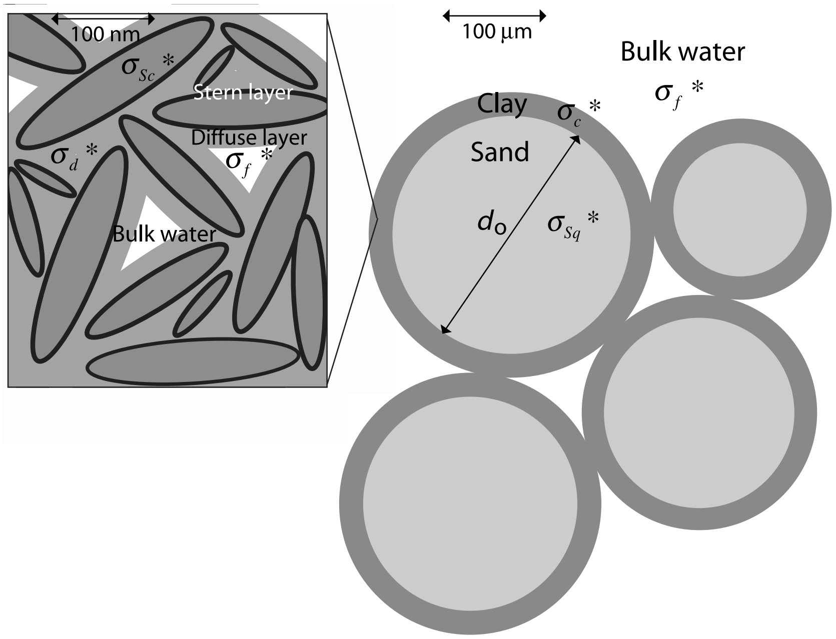

Figure 6. Sketch of the clay-sand mixtures for the modeling. The saturated clay of electric conductivity σ_c^* coats the spherical sand grains of surface conductivity σ_{Sq}^*. They are surrounded by the bulk pore water of conductivity σ_f^*. The saturated clay is constituted of elongated clay particles of surface conductivity σ_{Sc}^* surrounded by diffuse layer of conductivity σ_d^* and bulk pore water of conductivity σ_f^*.

$$\sigma_c^* \text{ updated to } \sigma_c^* + d\sigma_c^*, \tag{26}$$

$$\Omega_{Sc} \text{ updated to } \Omega_{Sc} + d\Omega_{Sc}, \tag{27}$$

where L is the depolarization coefficient of inclusions, which is calculated according to the value of the cementation exponent m (Mendelson and Cohen, 1982). In equations 25 and 27, the initial volume fraction of clay particles is equal to zero and the final volume fraction of inclusions is equal to $1 - \phi$ (ϕ is the porosity of pure clay samples).

The value of m (equation 24) depends on the aspect ratio of the clay particles. Leroy and Revil (2009) find that taking the following values (quartz, $m = 1.5$; kaolinite, $m = 2.0$; illite, $m = 3$; smectite, $m \in \{3,4\}$ depending on the aspect ratio of the particles; see Mendelson and Cohen, 1982) works well to predict the low-frequency complex conductivity of sands, clays, and clay-sand mixtures. The high value of the cementation exponent of smectite is justified by the high aspect ratio of the particles (Leroy and Revil, 2009; Tournassat and Appelo, 2011).

The complex surface conductivity of clay-sand mixtures σ_{Sm}^* is determined according to the coating clay model of Lima and Sharma (1990). In their model, clays are considered as a continuous conductive coating over the less conductive and spherical sand grains. Lima and Sharma (1990) obtain the following equation for the complex surface conductivity of clay-sand mixtures:

$$\sigma_{Sm}^* = \frac{\sigma_c^*[2\Omega_c\sigma_c^* + (3 - 2\Omega_c)\sigma_{Sq}^*]}{(3 - \Omega_c)\sigma_c^* + \Omega_c\sigma_{Sq}^*}, \tag{28}$$

where the subscript "Sq" refers to the complex surface conductivity of the quartz sand (including the effect of the PSD on the surface conductivity), respectively. Here, Ω_c is the volume fraction of the water-saturated coating clay and Ω_c is the ratio of the volume of water-saturated clay to the volume of saturated clay and dry sand grains.

Finally, the complex conductivity of the sample is also calculated using the DEM theory. The initial electric conductivity of the sample is the electric conductivity of the bulk pore water σ_f^*. Inclusions are clay-sand mixtures of surface conductivity σ_{Sm}^* and volume fraction $d\Omega_{Sm}$. The value of σ^* is calculated iteratively with equations 24–27 by replacing σ_c^* by σ^*, σ_{Sc}^* by σ_{Sm}^*, and Ω_{Sc} by Ω_{Sm}. The initial volume fraction of clay-sand mixtures is equal to zero, and the final volume fraction of inclusions is equal to $1 - \phi + \phi_c$, where ϕ is the porosity of the sample and ϕ_c is the porosity of the clays in the core sample (i.e., the porosity of pure clays multiplied by the volume fraction of water-saturated clays in the sample).

The complex surface conductivity model of the clay-sand mixture developed here depends on the volume fraction of water-saturated clays and uses the full DEM theory. Modeled clay particles have a high aspect ratio and sand grains are spherical. The pore space of water saturated clays contains diffuse layers (bentonite samples) or

Downloaded 11/18/14 to 138.67.11.98. Redistribution subject to SEG license or copyright; see Terms of Use at http://library.seg.org/

bulk pore water (kaolinite samples). The full DEM theory is also used to upscale the complex surface conductivity model to the complex conductivity model at the scale of the sample (pore water and grains). The parameters of our SIP model are summarized in Tables 3 and 4. In the next section, the predicted in-phase and quadrature conductivities of clays and clay-sand mixtures at different salinities will be compared to the corresponding measured complex conductivities.

COMPARISON BETWEEN THE EXPERIMENTAL DATA AND THE MODEL

Clay-sand mixtures in distilled water: impact of the clay mineralogy and clay content

The induced polarization model presented in this study can be used if the chemical composition of the bulk pore water is known. This is not the case of clay-sand mixtures immersed in distilled water because of partial dissolution of the minerals (Sverjensky, 2005) and hydrolysis of Na-montmorillonite (Delgado et al., 1986). Figure 7 shows the recorded in-phase and quadrature conductivity spectra of unconsolidated kaolinite-sand (K2 + S; K-type samples) and bentonite-sand (B2 + S; B-type samples) mixtures (see Table 1) for different clay contents and saturated with distilled water. Independently of the clay mineralogy (kaolinite or smectite), the highest values of the in-phase and quadrature conductivities are always observed for the 100% clay mixtures (no sand). In-phase and quadrature conductivities of bentonite-sand samples are always higher than those of kaolinite-sand samples (at given clay content) because of the higher surface conductivity of bentonites (Figure 7). Bentonites have considerably higher CEC than kaolinites (Table 1). Therefore, clay mineralogy and particularly their CEC affect strongly the complex conductivity response of clay-sand mixtures (Vinegar and Waxman, 1984).

The magnitude of the quadrature conductivity spectra of B-type samples is stronger than for the K-type samples. The very high smectite content of B2 bentonite (95 wt%, Table 1) is responsible for these observations. Smectites are characterized by their high permanent surface charge density, very high specific surface area, and also by their elongated form compared to kaolinites (Hassan et al., 2006; Leroy and Revil, 2009; Tournassat et al., 2011). As explained by Lockhart (1980) and Tombacz and Szekeres (2004), a smectite aggregate resembles a honeycomb of closed edge-to-face, edge-to-edge, and face-to-face units, whereas kaolinite tactoids are stacked as face-to-face units (Hassan et al., 2006; Leroy and Revil, 2009; Tombacz and Szekeres, 2006). Therefore, the distribution of relaxation times associated with the electrochemical polarization of the Stern layers around smectite particles is broader than that of the kaolinite particles. It results that the low-frequency quadrature conductivity spectra of smectites are broader than those of kaolinites.

The decrease of the quadrature conductivity spectra with the decrease of the clay content is more pronounced for K-type samples because of their lower CEC compared to B-type samples. Figure 7 clearly shows (in log scale) a shift of the measured quadrature conductivity spectra of K-type samples (relative to the measured maximum of quadrature conductivity at a given clay content) to lower frequencies when the clay content decreases. This can be explained by the progressive influence of the electrochemical polarization of larger sand grains on quadrature conductivity spectra of K2-sand mixtures (see equation 17, $f_0 \equiv 1/\tau_0 = 8k_bT\beta_i^{St}/ez_id_0^2$). The quadrature conductivity spectra of B-type samples shift (relative to the measured maximum of quadrature conductivity at a given clay content) to higher frequencies when the clay content decreases. Even at a very low clay content (1%), because of the high CEC of bentonites,

Table 3. Nomenclature of the material properties.

Symbol	Meaning	Unit
ϕ	Total porosity	Dimensionless
Z	Impedance of the sample	Ω
ρ	Resistivity of the sample	$\Omega\,\mathrm{m}$
K	Geometric factor of the sample	m
φ	Phase of the sample	rad
σ	Electric conductivity of the sample	$\mathrm{S\,m^{-1}}$
σ_c	Electric conductivity of the saturated coating clay	$\mathrm{S\,m^{-1}}$
σ_S	Surface electric conductivity	$\mathrm{S\,m^{-1}}$
σ_{Sm}	Surface electric conductivity of the mixture	$\mathrm{S\,m^{-1}}$
σ_{Sc}	Surface electric conductivity of the clay	$\mathrm{S\,m^{-1}}$
σ_{Sq}	Surface electric conductivity of the quartz sand	$\mathrm{S\,m^{-1}}$
σ_w	Electric conductivity of the clay pore water	$\mathrm{S\,m^{-1}}$
σ_f	Electric conductivity of the bulk pore water	$\mathrm{S\,m^{-1}}$
σ_d	Electric conductivity of the diffuse layer	$\mathrm{S\,m^{-1}}$
Ω_c	Volume fraction of water saturated clay	Dimensionless
Ω_{Sm}	Volume fraction of water saturated clay-sand mixtures	Dimensionless
Ω_{Sc}	Volume fraction of clay particles	Dimensionless
ε_g	Grain dielectric permittivity	$\mathrm{F\,m^{-1}}$
d_0	Grain diameter	m
$f(d_{0i})$	Grain size distribution	Dimensionless
Q_V	Volumetric charge density of the pore space	$\mathrm{C\,m^{-3}}$
Q_0	Surface charge density of the mineral	$\mathrm{C\,m^{-2}}$
Q_{St}	Surface charge density of the Stern layer	$\mathrm{C\,m^{-2}}$
Q_d	Surface charge density of the diffuse layer	$\mathrm{C\,m^{-2}}$
ρ_g	Grain volumetric density	$\mathrm{kg\,m^{-3}}$
ϕ_c	Clay porosity in the sample	Dimensionless
S_s	Specific surface area	$\mathrm{m^2\,g^{-1}}$
CEC	Cation exchange capacity	$\mathrm{meq\,g^{-1}}$
m	Cementation exponent	Dimensionless
F	Formation factor	Dimensionless
L	Depolarization coefficient	Dimensionless

Downloaded 11/18/14 to 138.67.11.98. Redistribution subject to SEG license or copyright; see Terms of Use at http://library.seg.org/

quadrature conductivity spectra of B2-sand mixtures may still be dominated by the electrochemical polarization of the clay. The decrease of the size of the B2-clay aggregates with the decrease of the clay content may explain the shift of the quadrature conductivity spectra to higher frequencies.

Table 4. Nomenclature of the other parameters and constants.

Symbol	Meaning	Unit
ω	Angular frequency	rad s^{-1}
f	Frequency	Hz
ψ_m	Donnan potential	V
e	Elementary charge of the electron	C
N_A	Avogadro number	mol^{-1}
z_i	Valence of ion i	Dimensionless
C_i^d	Ion concentration in the diffuse layer	mol dm^{-3}
C_i^f	Ion concentration in the bulk pore water	mol dm^{-3}
k_b	Boltzmann constant	J K^{-1}
T	Temperature	K
I	Ionic strength	mol dm^{-3}
f_Q	Partition coefficient between Stern and diffuse layer charges	Dimensionless
Γ_i^d	Surface site density of adsorbed ions in the diffuse layer	m^{-2}
Γ_i^{St}	Surface site density of adsorbed ions in the Stern layer	m^{-2}
β_i^f	Ion mobility in the bulk pore water	$\text{m}^{-2}\,\text{s}^{-1}\,\text{V}^{-1}$
β_i^d	Ion mobility in the diffuse layer	$\text{m}^{-2}\,\text{s}^{-1}\,\text{V}^{-1}$
β_i^{St}	Ion mobility in the Stern layer	$\text{m}^{-2}\,\text{s}^{-1}\,\text{V}^{-1}$
χ_d	Debye length	m
ε_f	Bulk water dielectric permittivity	F m^{-1}
ε_d	Diffuse layer dielectric permittivity	F m^{-1}
ε_r	Relative dielectric permittivity	Dimensionless
ε_0	Vacuum dielectric permittivity	F m^{-1}
Σ_S^0	Total specific surface conductivity of the mineral	S
Σ_S^{St}	Specific surface conductivity of the Stern layer	S
Σ_S^d	Specific surface conductivity of the diffuse layer	S
τ_0	Relaxation time	s
f_0	Characteristic frequency	Hz

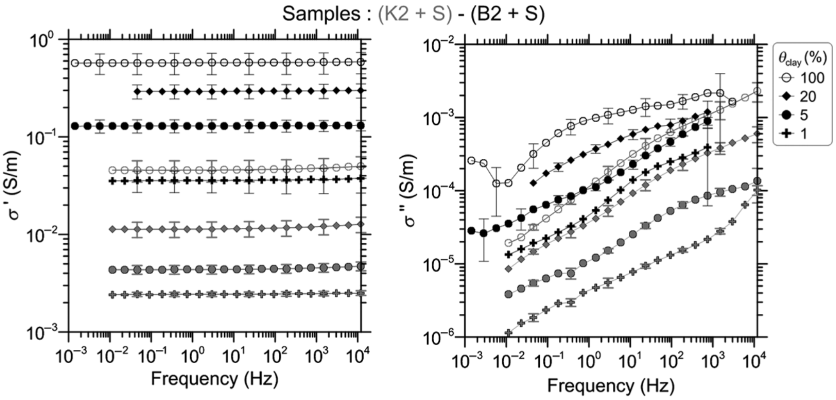

Figure 7. Comparison of the in-phase and quadrature conductivity spectra of clay-sand mixtures composed of kaolinite (K2) and smectite (B2) for varying clay contents. All samples are saturated with distilled water. The error bars correspond to twice the standard deviation computed on three cycles at each frequency.

Figure 8 shows the measured in-phase and quadrature conductivities of the two kaolinite-sand mixtures (K1 + S) and (K2 + S) saturated with distilled water. The in-phase and quadrature conductivities of these mixtures are similar (mostly inside the error bars of the measurements) at a given clay content and frequency. Nevertheless, conductivity spectra of (K1 + S) mixtures are overall higher than those of (K2 + S) mixtures (except the in-phase conductivity of the pure clays samples) because K1 contains a significant fraction of smectites (15 wt%; Table 1). This is particularly the case for the quadrature conductivity of the samples with 1% clay content (in volume) at low frequencies (<100 Hz).

Figure 9 shows the in-phase and quadrature conductivities of the two bentonite-sand mixtures (B1 + S) and (B2 + S) saturated with distilled water. The in-phase conductivities of the two pure clay samples are roughly the same (inside the error bars of the measurements) but the in-phase and quadrature conductivities of mixtures (B2 + S) (at a given clay content and frequency) are always higher than those of mixtures (B1 + S). The mineralogy of the two bentonites is roughly the same, as revealed by the XRD analyses (95 wt% of smectite and 5 wt% of kaolinite; see Table 1). The observed difference in conductivities may be related to the slightly higher CEC of samples (B2 + S) (the CEC of B2 is 0.442 meq g^{-1}, whereas the CEC of B1 is 0.34 meq g^{-1}), which is therefore responsible for a higher surface conductivity.

In addition, Figure 10 is also plotted to observe the effect of the clay content on the in-phase and quadrature conductivity at a given frequency (here, 1.46 Hz is chosen). Figure 10 illustrates clearly that, at 1.46 Hz, independently from clay mineralogy (K1, K2 or B1, B2), in-phase and quadrature conductivity increase in a similar way when the clay volume fraction increases. This increase is highest for B2 clay that has the highest CEC. Bentonite-sand mixtures have considerably higher in-phase conductivities than kaolinite-sand mixtures. Quadrature conductivities of B1-sand mixtures are significantly lower than quadrature conductivities of B2-sand mixtures. Therefore, the increase of the in-phase and quadrature conductivities of clay-sand mixtures with the clay content is strongly associated with the CEC of clay.

Clay-sand mixtures in saline waters: Impact of the clay mineralogy, clay content, and salinity

Figures 11 and 12 display the in-phase and quadrature conductivities of kaolinite-sand (K1+

Downloaded 11/18/14 to 138.67.11.98. Redistribution subject to SEG license or copyright; see Terms of Use at http://library.seg.org/

S) and bentonite-sand (B2 + S) mixtures saturated with NaCl aqueous electrolytes at different salinities. Note that we obtained very noisy spectra for the samples with the lowest clay content (1%) and saturated with the highest salinities (pore water electric conductivities of 15 and 18 $\mathrm{mS\,cm^{-1}}$) because of the very low values of the phase at these salinities, close to the detectability limit of the instrument. Figure 11 shows that the magnitude of the in-phase conductivity of K1-sand mixtures increases significantly with salinity because of the low surface conductivity of the clay and the resulting strong influence of the bulk pore water electric conductivity. The (DC) surface conductivity is associated with electromigration currents in the Stern and diffuse layers around particles (Revil and Glover, 1997). It increases slightly with salinity compared to the bulk water electric conductivity (Leroy et al., 2012; 2013), in particular for minerals with a constant surface charge density such as smectite (Leroy and Revil, 2004).

The quadrature conductivity of K1-sand samples is fairly independent on salinity (it increases slightly with salinity) at high clay contents (higher or equal to 20%), probably because of the constant CEC and surface charge density of smectite (the weight fraction of smectite in K1-clay is equal to 15%; Table 1). Quadrature conductivity spectra of K1-sand mixtures are therefore less sensitive than their in-phase conductivity spectra to salinity. In addition, their amplitude increases with the frequency due to electrochemical polarization of the Stern layers around particles with different sizes.

Nevertheless, the quadrature conductivity of K1-sand mixtures increases significantly with the salinity at a very low clay content (1% of the sample volume) in which the electrochemical properties of the sand may compete with the electrochemical properties of the clay (Figure 11). The magnitude of the surface charge density of the sand increases with salinity and is responsible for the development of a Stern layer (Sahai and Sverjensky, 1997; Sverjensky, 2005). The surface site densities of adsorbed counterions in the Stern layer of silica rise with salinity and may be responsible for the observed increase of the quadrature conductivity (Leroy et al., 2008).

Figure 12 shows that the surface conductivity of B2-sand mixtures is significantly higher than the surface conductivity of K1-sand mixtures. It results that the in-phase conductivity of B2-sand mixtures is slightly dependent on salinity, except in the case of the lowest clay content (1% of the sample volume) because of its low surface conductivity. Quadrature conductivity of bentonite-sand mixtures is fairly independent on salinity (it increases slightly with salinity, except for the mixture with 1% clay content) because of

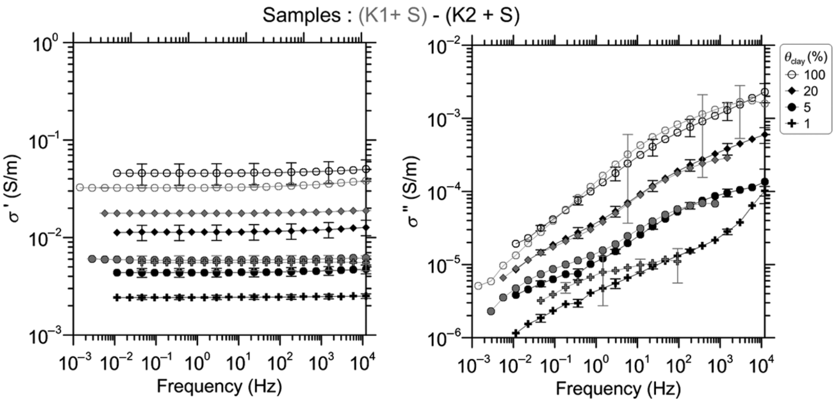

Figure 8. Comparison of the in-phase and quadrature conductivity spectra of clay-sand mixtures composed of two kaolinite clays (K1 and K2) for varying clay contents. All samples are saturated with distilled water. The error bars correspond to twice the standard deviation computed on three cycles at each frequency.

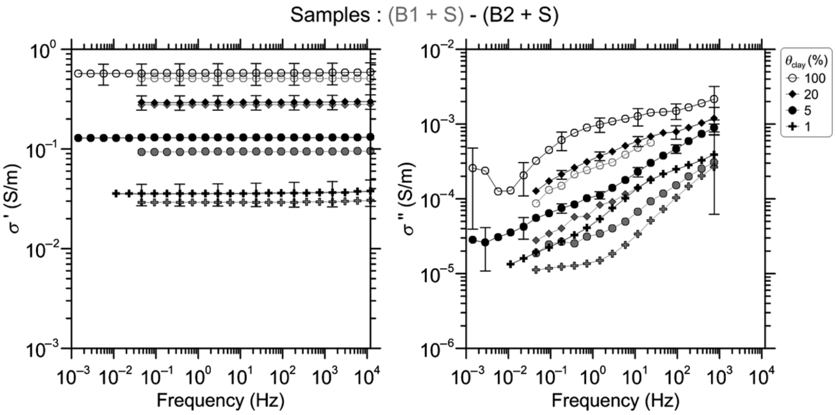

Figure 9. Comparison of the in-phase and quadrature conductivity spectra of clay-sand mixtures composed of two bentonite clays (B1 and B2) for varying clay contents. All samples are saturated with distilled water. The error bars correspond to twice the standard deviation computed on three cycles at each frequency.

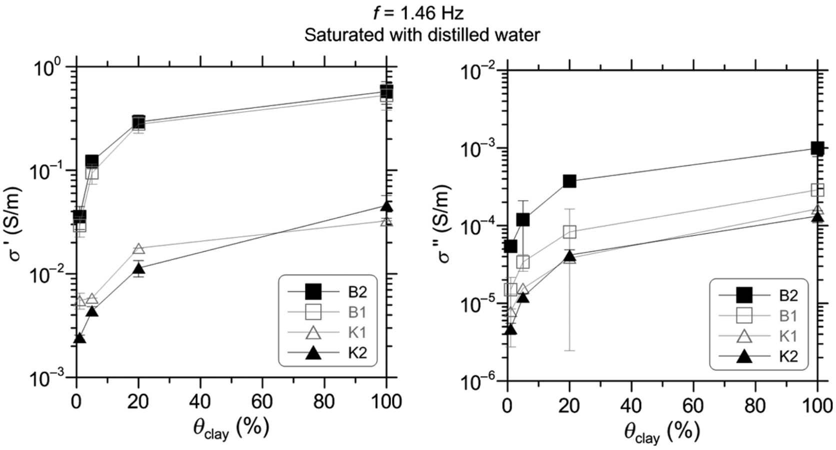

Figure 10. Effect of the clay content (θ_{clay}) on the in-phase (σ') and quadrature conductivity (σ'') at 1.46 Hz for various clay-sand mixtures prepared with bentonite (B1, B2) and kaolinite (K1, K2) clays and saturated with distilled water (different clay volume fractions of 100%, 20%, 5%, and 1%).

Downloaded 11/18/14 to 138.67.11.98. Redistribution subject to SEG license or copyright; see Terms of Use at http://library.seg.org/

the high CEC of smectite. The quadrature conductivity of the B2-sand mixture with the lowest clay content is less dependent on salinity than the quadrature conductivity of the K1-sand mixture with the lowest clay content (measured data at the highest salinities cannot be used because of the inaccuracy of the measurements).

In Figure 13, we summarize the effect of the clay mineralogy, content, and salinity of the bulk pore water on the magnitude of the in-phase and quadrature conductivities. This figure shows different sets of (K + S) and (B + S) mixtures with 20% or 5% volumetric clay fraction. These intermediate percentages of volumetric clay fraction have been chosen for two reasons: (1) the availability of all ranges of fluid salinities for these clay contents independent to instrumental limitation on the measurement of the phase and (2) our preference to maintain mixtures having a relatively high concentration of clay minerals to focus on clayey materials rather than on sandy materials. Figure 13 shows that the in-phase and quadrature conductivities of (B+S) samples are considerably higher than those of (K + S) samples. The results presented in Figure 13 also demonstrate that the magnitude of the in-phase conductivity of the kaolinite-sand samples is strongly dependent to saturating fluid salinity for all volumetric clay fractions. Therefore, the in-phase conductivity of the (K + S) samples increases strongly with the salinity except at very low salinities of 0.0017 mol L^{-1} NaCl for which surface conductivity may dominate the bulk pore water electric conductivity.

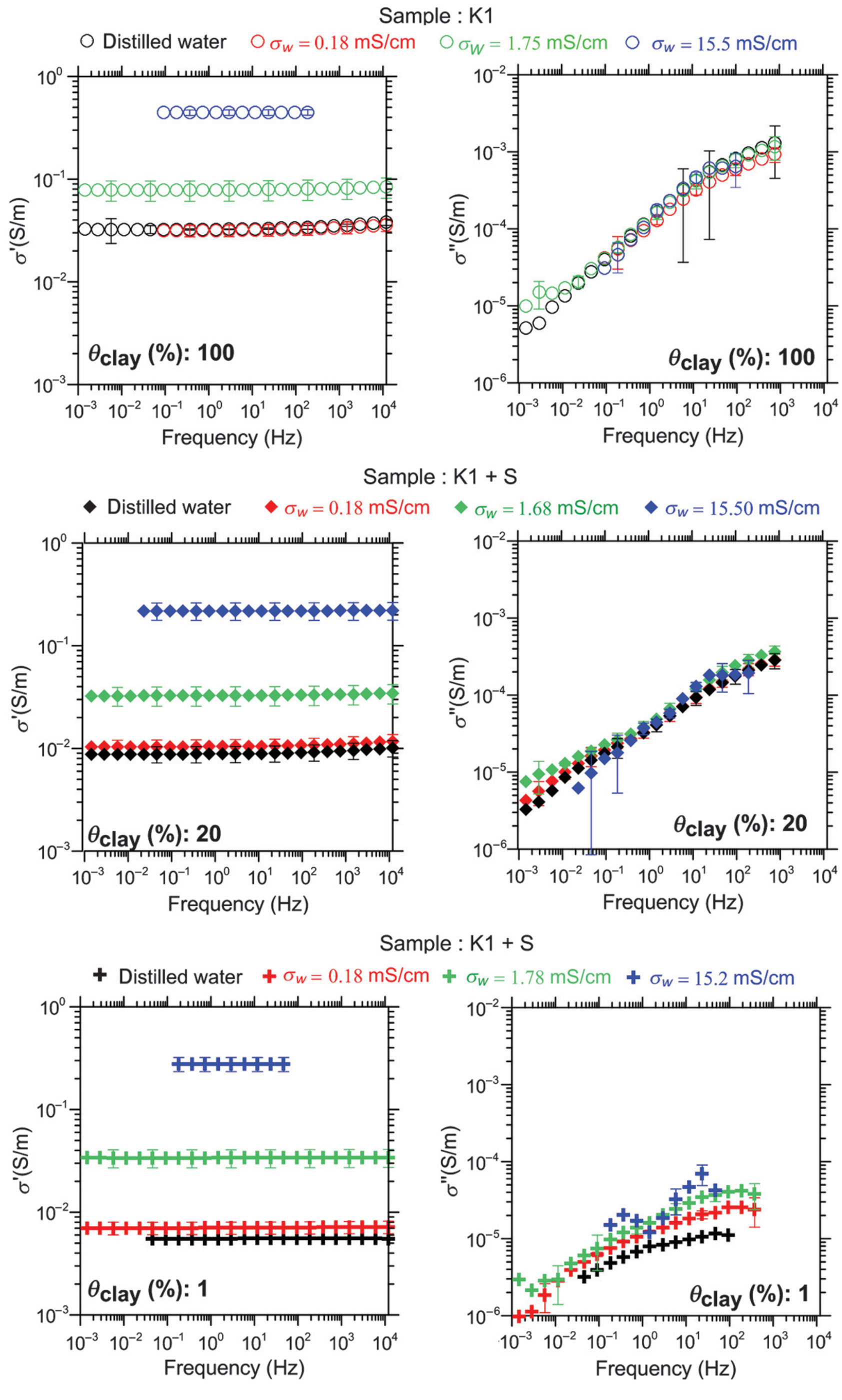

Figure 11. In-phase and quadrature conductivity spectra of clay-sand mixtures (K1 + S) for different saturating fluid salinities (NaCl) and clay contents. The error bars correspond to twice the standard deviation computed on three cycles at each frequency.

Figure 14 is plotted additionally to observe the effect of the salinity on the in-phase and quadrature conductivities at a given frequency (here, 1.46 Hz is chosen) and at various clay contents (100%, 20%, 5%, and 1% of the sample volume). In the case of the (B + S) mixtures, the in-phase conductivity increases slightly with salinity (except for the low clay contents of 1% and 5% for which the in-phase conductivity increases greatly with the salinity). This is also consistent with the high CEC of smectite and therefore the strong effect of its surface conductivity. Regarding the quadrature conductivity, the magnitude of the polarization increases slightly with salinity because it is also principally controlled by the CEC of clays, as discussed by Vinegar and Waxman (1984), Revil (2012), and Revil et al. (2013a, 2013b) for clayey sandstones and saprolites. The difference of porosity from one sample to the other could play a secondary role in the difference of quadrature conductivity. Therefore, the (B + S) mixtures, at a given frequency and clay content, are expected to have higher in-phase and quadrature conductivities than the (K+S) mixtures. In the next section, complex conductivity spectra of clays and clay-sand mixtures at different clay contents and salinities are modeled using our induced polarization model.

Complex conductivity modeling

Surface site densities of adsorbed ions in the Stern and diffuse layers, Γ_i^d and Γ_i^{St}, are calculated using the Donnan equilibrium model (equations 4, 7 or 8, 10–13). The surface site density of adsorbed ions in the diffuse layer is calculated for a layer of thickness $\Delta \approx 2\chi_d$ (equation 10). The fitting parameters are the partition coefficient between the surface charge densities of the Stern and diffuse layers f_Q and the excess of charge

Downloaded 11/18/14 to 138.67.11.98. Redistribution subject to SEG license or copyright; see Terms of Use at http://library.seg.org/

per unit pore volume Q_V. Q_V is calculated using volumetric grain density ρ_g, porosity ϕ, the product of the specific surface area S_s by the surface charge density Q_0 (sand; equation 7) or CEC (clays; equation 8). The complex surface conductivity of clays σ^*_{Sc} and of quartz sand σ^*_{Sq} is calculated according to the computed values of Γ_i^d and Γ_i^{St} and equations 14–20. The discretized PSD $f(d_{0i})$ and the surface mobility of counterions in the Stern layer β_i^{St} are the two key parameters of these equations. The electric conductivity of the pore water of bentonite $\sigma^*_w = \sigma^*_d$ is computed using equation 23. The electric conductivity of the bulk pore water of kaolinite $\sigma^*_w = \sigma^*_f$ is taken from the measured values. The DEM theory (equations 24–27) is also used for the calculation of the complex conductivity of water-saturated clay aggregates σ^*_c knowing σ^*_w and σ^*_{Sc}. Kaolinite and smectite particles are initially assumed slightly ($m = 2$) and highly ($m = 4$) elongated, respectively. The complex surface conductivity of clay-sand particles σ^*_{Sm} is determined according to the coating clay model (equation 28) with the computed values of σ^*_{Sq} and σ^*_c, and the volumetric (water-saturated) clay fractions. Finally, the complex conductivity of the sample is modeled using the DEM theory and computed values of σ^*_{Sm} and σ^*_f. Measured in-phase conductivities of clays and clay-sand mixtures immersed in a saline water ($C^f_{\mathrm{NaCl}} = 0.017$ mol L^{-1} and $C^f_{\mathrm{NaCl}} = 0.17$ mol L^{-1}), porosities (Table 2), our induced polarization model, and Archie's law ($F = \phi^{-m}$; Archie, 1942) are used to estimate the cementation exponents of clays and clay-sand mixtures and the resulting formation factor. Nevertheless, in the case of B2-bentonite, we have not enough conductivity measurements (only for distilled and low salinity water, $C^f_{\mathrm{NaCl}} = 0.0017$ mol L^{-1}) to estimate the formation factor. B2-bentonite contains 95% of smectite (in weight percentage; Table 1). Therefore, like Leroy and Revil (2009), we use $m = 4$ to model the complex conductivity of B2-clay. The resulting formation factor is estimated using measured porosity and Archie's law.

The mobility of sodium and chloride ions in bulk pore water $\beta^f_{\mathrm{Na}^+}$ and $\beta^f_{\mathrm{Cl}^-}$ are taken equal to 5.19×10^{-8} and 7.89×10^{-8} m^2 s^{-1} V^{-1}, respectively (Turq et al., 1969). The volumetric grain density ρ_g of silica is 2650 kg m^{-3} (Baba and Komar, 1981), and the volumetric grain densities of kaolinite, smectite, and illite, are taken as equal to 2600 kg m^{-3}, 2700 kg m^{-3}, and 2800 kg m^{-3}, respectively (Leroy and Revil, 2009). Therefore, according to the measured clays mineralogy (Table 1), the theoretical volumetric grain densities of K1- and B2-clays are equal to 2625 kg m^{-3} and 2695 kg m^{-3}, respectively. We test two assumptions for the sodium ion mobility in the Stern layer of clays: (1) $\beta^{St}_{Na^+} = \beta^f_{Na^+}/2$ (Tournassat et al., 2009; Bourg and Sposito, 2011), and (2) $\beta^{St}_{Na^+} = \beta^f_{Na^+}/350$ (Revil, 2012; Revil et al., 2013a, 2013b). The sodium ion mobility in the Stern layer of silica is assumed to be very close to its value in the bulk pore water because sodium ions are adsorbed as outer-sphere complexes (Leroy et al., 2013).

The effect of the PSD on the complex conductivity spectra is modeled with a Cole-Cole distribution (Leroy and Revil, 2009). The Cole-Cole distribution is given by

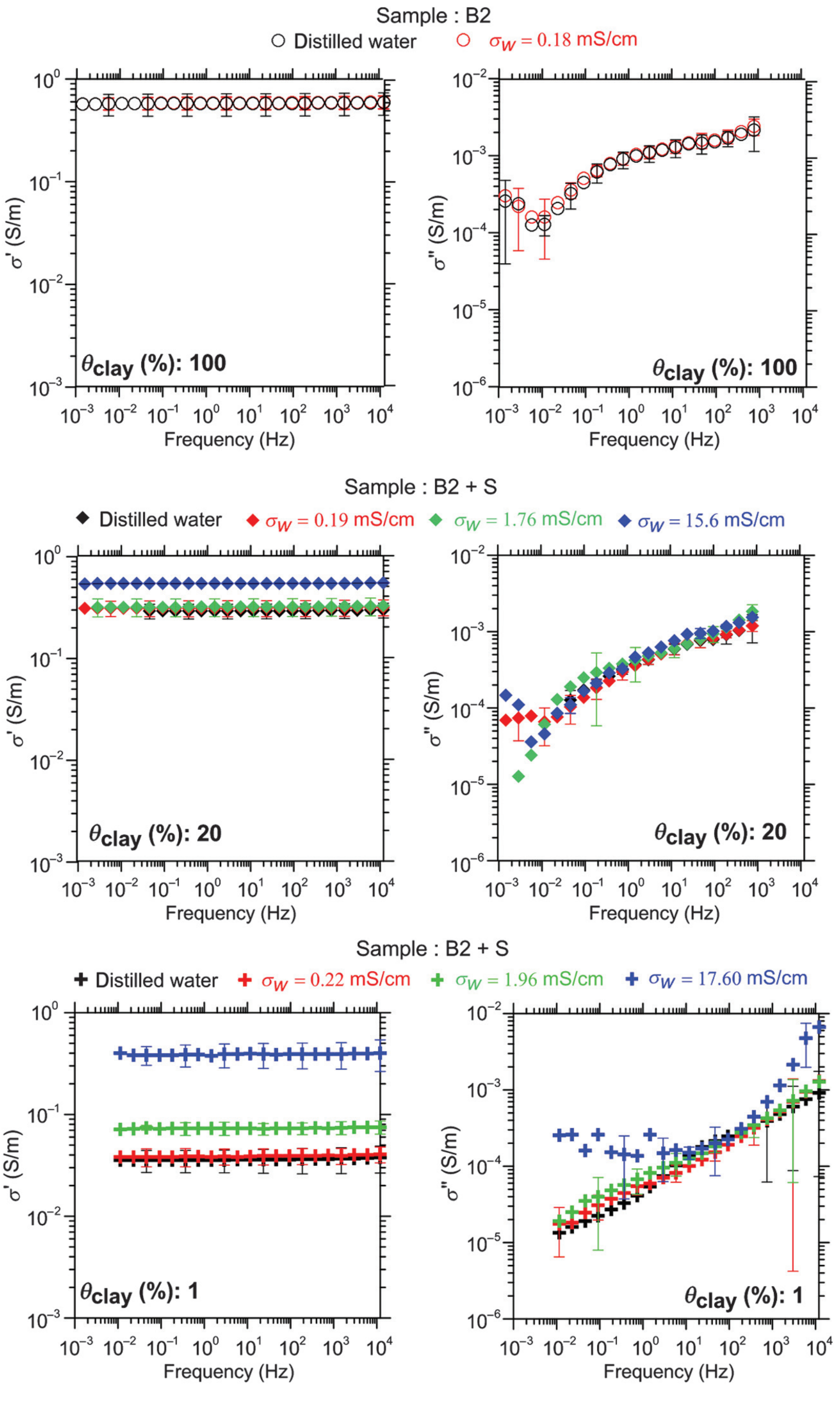

Figure 12. In-phase and quadrature conductivity spectra of clay-sand mixtures (B2 + S) for different saturating fluid salinities (NaCl) and clay contents. The error bars correspond to twice the standard deviation computed on three cycles at each frequency.

Downloaded 11/18/14 to 138.67.11.98. Redistribution subject to SEG license or copyright; see Terms of Use at http://library.seg.org/

$$f(d_0)=\frac{1}{\pi d_0}\frac{\sin[\pi(1-c)]}{\cosh[2c\ln(d_0/d_{50})]-\cos[\pi(1-c)]}, \tag{29}$$

where d_{50} represents the median of the polarization length scale distribution and c is the Cole-Cole exponent ($0 \leq c \leq 1$). The case $c = 1$ corresponds to a Debye model.

K1-clay and K1-sand mixtures

On the contrary to B2-clay in which a significant CEC was measured (Table 1), the CEC of kaolinite K1 was fitted according to complex conductivity spectra. The predicted in-phase and quadrature conductivities of K1-clay and K1-sand mixtures are in fairly good agreement with the experimental data, except at low frequencies ($<10^{-1}$ Hz) at which membrane polarization may occur (Figure 15). As explained by Lesmes and Morgan (2001) and more recently by Revil and Florsch (2010), our SIP model does not consider the polarization due to the diffusion of counterions over multiple grain lengths on the complex conductivity response. Predictions of complex conductivity spectra using the two assumptions (for the sodium ion mobility in the Stern layer of clays) give similar results, except that assumption (2) leads to smaller modeled particles sizes, higher f_Q and CEC than assumption (1) (Tables 5 and 6). With the assumption $\beta^{St}_{\mathrm{Na}^+} = \beta^{f}_{\mathrm{Na}^+}/2$, the median diameter of the modeled PSD of pure K1-clay corresponds to the measured median diameter of clay aggregates in vacuum (Figure 15). This means that the Stern layers around clay aggregates may control the in-phase and quadrature conductivity responses of the pure K1-clay and K1-sand mixtures (except of the mixture with a very low clay content of 1%). With the assumption $\beta^{St}_{\mathrm{Na}^+} = \beta^{f}_{\mathrm{Na}^+}/350$, the modeled particles sizes of pure K1-clay are considerably smaller than those of quartz sand, in agreement with the assumption that clay particles have sizes in the range of the micrometer or smaller whereas fine quartz particles have sizes in the range of hundreds of micrometers to millimeters (Lima and Sharma, 1990, Lesmes and Morgan, 2001; Leroy et al., 2008; Leroy and Revil, 2009; Tournassat et al., 2011). The modeled characteristic frequency f_0 depends on the ratio of the surface mobility of the sodium counterions in the Stern layer β^{S}_{Na} to the square of the particle diameter d_0 (equation 17; $f_0 \equiv 1/\tau_0 = 8k_bT\beta^{St}_{\mathrm{Na}}/ed_0^2$). If β^{S}_{Na} decreases from $\beta^{St}_{\mathrm{Na}^+} = \beta^{f}_{\mathrm{Na}^+}/2$ to $\beta^{St}_{\mathrm{Na}^+} = \beta^{f}_{\mathrm{Na}^+}/350$, d_0 must decrease from d_0 to $d_0/\sqrt{175}$, to model identical characteristic frequencies. According to equations 14–16, the magnitude of conduction and polarization current densities in the Stern layer decreases with the diminution of β^{S}_{Na}. This explains the increase of the partition coefficient f_Q and excess of charge per unit pore volume Q_V (through estimated CEC, equation 8) if β^{S}_{Na} decreases from $\beta^{St}_{\mathrm{Na}^+} = \beta^{f}_{\mathrm{Na}^+}/2$ to $\beta^{St}_{\mathrm{Na}^+} = \beta^{f}_{\mathrm{Na}^+}/350$.

Tables 5 and 6 show that the high conductivity spectra of pure K1-clay compared to those of the mixture are mainly due to the low formation factor and high CEC of the sample K1 compared to the higher formation factor and lower specific surface area and surface charge densities (at low salinities) of the quartz sand. The estimated values of the partition coefficient of K1-clay show that most adsorbed ions are located in the Stern layer, in agreement with the values calculated by Leroy and Revil (2009). Estimated f_Q values of the sand are significantly lower than the estimated f_Q values of pure K1-clay. This can be explained by the presence of silica lowering considerably the partition coefficient. The increase of magnitude of the surface charge density of silica with salinity is responsible for an increase of the surface site densities of adsorbed counterions in the Stern layer, and therefore to an increase of the partition coefficient (Leroy et al., 2008; Leroy et al., 2013).

The estimated CEC of pure K1-clay remains constant, in accordance with our assumption that its electrochemical conduction and polarization are dominated by smectite (Tables 5 and 6). However, the CEC values found (0.18 meq g^{-1} for $\beta^{St}_{\mathrm{Na}^+} = \beta^{f}_{\mathrm{Na}^+}/2$ and 1.4 meq g^{-1} for $\beta^{St}_{\mathrm{Na}^+} = \beta^{f}_{\mathrm{Na}^+}/350$) are considerably higher than the measured value (CEC < 0.1 meq g^{-1}; Table 1) and the value reported by Revil and Leroy (2004) for kaolinite (CEC = 0.05 ± 0.03 meq g^{-1}). The very high estimated CEC can be explained by the presence of smectite (CEC = 1 meq g^{-1} on average; Revil and Leroy, 2004). By using the mineralogical composition of K1-clay (80% of kaolinite, 15% of smectite, and 5% of illite-muscovite, in weight percentage; Table 1) and the average CEC of kaolinite (0.05 meq g^{-1}),

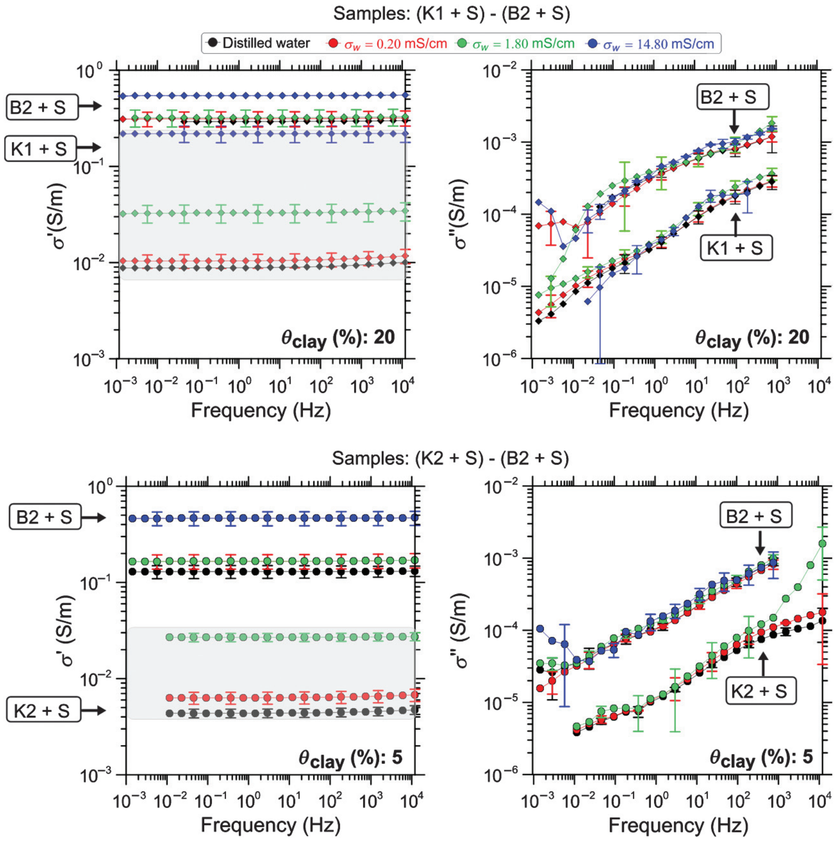

Figure 13. In-phase and quadrature conductivities for different clay mineralogies (kaolinite and smectite), clay contents (20%, 5%), and pore water salinities. The error bars correspond to twice the standard deviation computed on three cycles at each frequency. The gray area on the left-side of these figures corresponds to the data for the kaolinite-sand mixtures.

Downloaded 11/18/14 to 138.67.11.98. Redistribution subject to SEG license or copyright; see Terms of Use at http://library.seg.org/

smectite (1 meq g^{-1}), and illite (0.2 meq g^{-1}) (reported by Revil and Leroy, 2004), we calculate a theoretical CEC of 0.2 meq g^{-1} for pure K1-clay. This CEC value is very close to the estimated value using $\beta_{Na^+}^{St} = \beta_{Na^+}^{f}/2$ (0.18 meq g^{-1}). When using equation 10, we also have assumed that the mean pore size of the materials is equal to four Debye lengths. This is formally exact when the electric double layer occupies all the pore space of the material (Revil and Leroy, 2004). In reality, the mean pore size is certainly significantly larger because, in a clay-rich porous medium, a significant volume of bulk pore water and interlayer water still exists (Tournassat and Appelo, 2011). These explanations may explain why the CEC values of our SIP model are higher than the measured value. This may also explain the very high CEC found by using $\beta_{Na^+}^{St} = \beta_{Na^+}^{f}/350$ (1.4 meq g^{-1}). The estimated magnitudes of the surface charge density of the Fontainebleau sand are higher (but in the same order of magnitude) than the values reported by Sahai and Sverjensky (1997) for natural quartz immersed in a neutral and saline aqueous solution (NaCl). On the contrary to clay aggregates, quartz sands are usually not microporous and their interior can therefore be considered nonconducting. But, the Donnan equilibrium model may underestimate the surface site densities of ions in the Stern and diffuse layer because of the assumption $\Delta \approx 2\chi_d$ (equation 10).

The modeled PSDs of the smallest particles of K1-clay and sand are significantly broader than those measured in vacuum using a laser granulometer ($\beta_{Na^+}^{St} = \beta_{Na^+}^{f}/2$; Figure 15). As explained by Lesmes and Morgan (2001), the primary reason for this is that the complex electric conductivity measurements are sensitive to the size, shape, and surface roughness of the particle, whereas the measured PSD is only sensitive to the effective size of the particle. Relaxation of counterions around the Stern layers of clay tactoids and surface roughness of sand influence the complex conductivity response of the sample, whereas the particle size measurement is rather sensitive to large particles. As emphasized by Leroy et al. (2008), surface roughness of the particle can lead to larger quadrature conductivity spectra.

B2-clay and B2-sand mixtures

We model now the complex conductivity of pure B2-bentonite and bentonite-sand (B2 + S) mixtures with varying clay contents (1% and 20% in volume). The predicted in-phase and quadrature conductivities of B2-clay and B2-sand mixtures are in fairly good agreement with the experimental data, except at low frequencies (<10^{-1} Hz) at which membrane polarization may

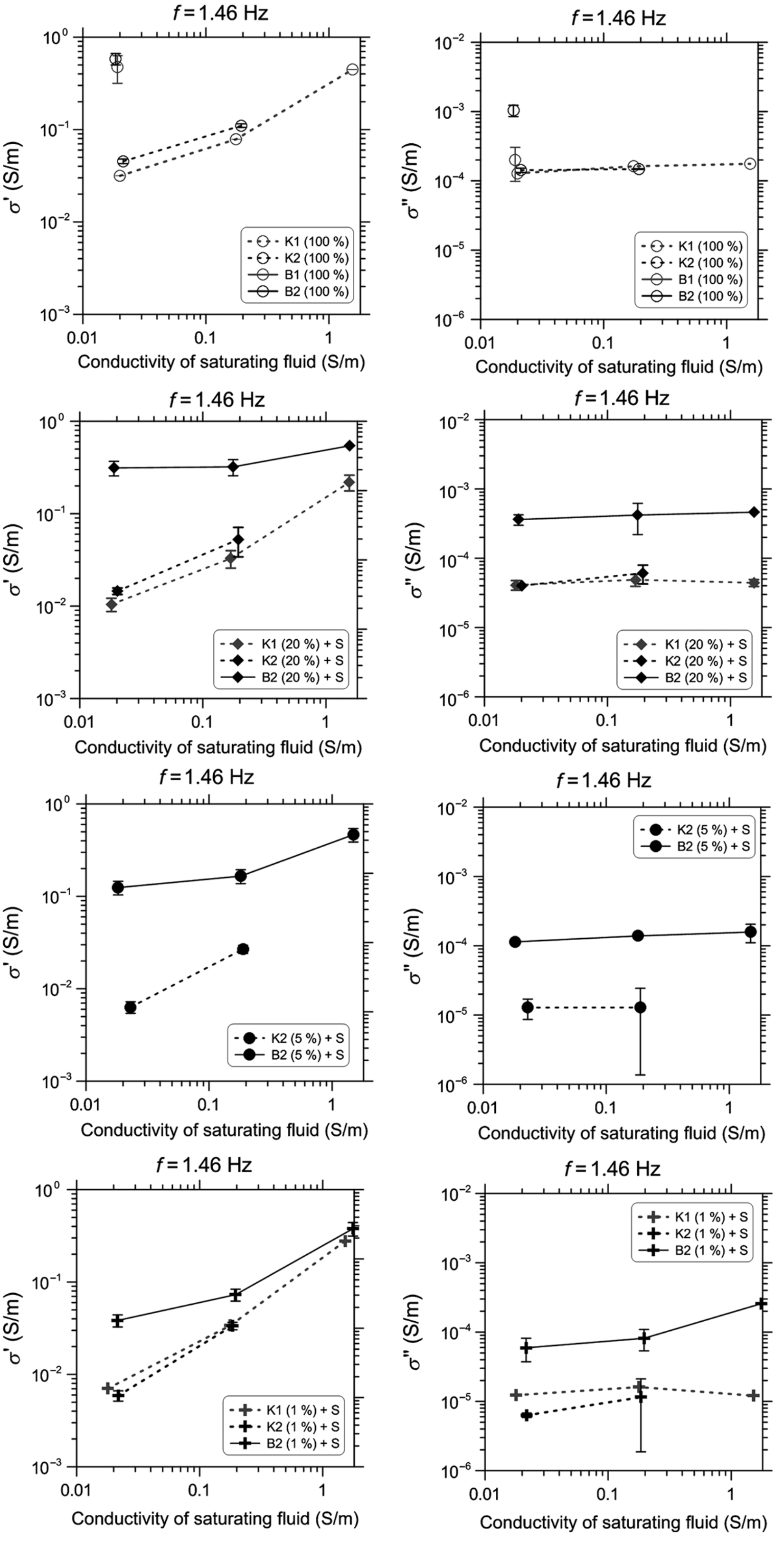

Figure 14. Effect of the salinity on the in-phase and quadrature conductivity at 1.46 Hz for various clay-sand mixtures prepared with bentonite (B1, B2) and kaolinite (K1, K2) clays (different clay volume fractions of 100%, 20%, 5%, and 1%).

Downloaded 11/18/14 to 138.67.11.98. Redistribution subject to SEG license or copyright; see Terms of Use at http://library.seg.org/

occur (Figure 16). Like K1-clay and K1-sand mixtures, predictions of complex conductivity spectra using the two assumptions (for the sodium ion mobility in the Stern layer of clays) give similar results, except that assumption (2) leads to smaller modeled particles sizes and higher f_Q and CEC than assumption (1) (Tables 7 and 8).

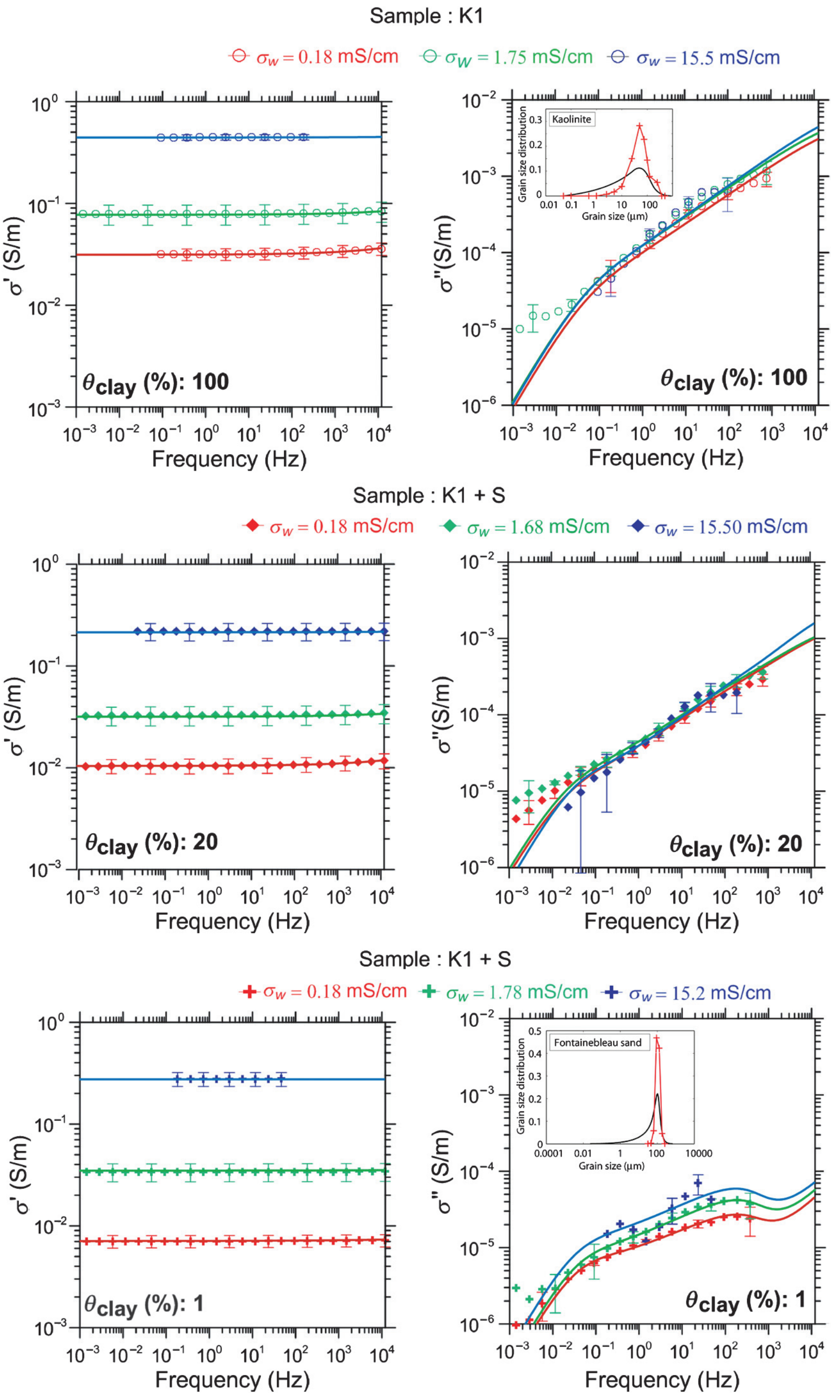

Figure 15. Modeled (lines) in-phase and quadrature conductivity spectra of clay-sand mixtures (K1 + S) for different saturating fluid salinities and clay contents (symbols: measurements). The modeled grain size distribution is represented by the black line in the upper right hand corner (symbols: measurements in vacuum).

The formation factors F of the bentonite-sand mixtures determined from in-phase conductivity measurements are provided in Tables 7 and 8. These values cannot explain the considerably higher in-phase and quadrature conductivities of B2 and B2-sand mixtures than the in-phase and quadrature conductivities of K1 and K1-sand mixtures (especially for the in-phase conductivity at low salinity). Only the difference in CEC between B2 and K1 can explain these observations. In addition, in the induced polarization model, the porosity of the B2-bentonite was significantly reduced to reproduce the recorded complex conductivity spectra of B2-sand mixtures. With the assumption $\beta^{St}_{\mathrm{Na}^+} = \beta^{f}_{\mathrm{Na}^+}/2$, the porosities of B2-bentonite were taken equal to 0.67, 0.10, and 0.05 for 100%, 20%, and 1% of B2 bentonite, respectively. With the assumption that $\beta^{St}_{\mathrm{Na}^+} = \beta^{f}_{\mathrm{Na}^+}/350$, the porosities of B2 bentonite were taken equal to 0.27, 0.05, 0.025 for 100%, 20%, and 1% of B2-bentonite, respectively. We explain the decrease of the porosity of B2-bentonite with the increase of the sand content by the resulting increase of the compaction of the clay and the formation of the interlayer pore space (Tournassat and Appelo, 2011). In the interlayer pore space, relaxation of counterions occurs at considerably higher frequencies compared to the frequencies investigated in our study (typically for frequencies > MHz, Cadène et al., 2006).

The values of the partition coefficient of B2-bentonite show that most adsorbed ions are located in the Stern layer, in agreement with the values calculated by Leroy and Revil (2009) for clays. The f_Q values of B2-clay are lower than the f_Q values of K1-clay. This can be explained by the higher kaolinite content of K1-clay, which increases the percentage of counterions in the Stern layer (Leroy and Revil, 2009). Finally, with the assumption that $\beta^{St}_{\mathrm{Na}^+} = \beta^{f}_{\mathrm{Na}^+}/2$, the modeled PSD of homogeneous B2-bentonite is very close to the measured PSD in vacuum (Figure 16).

DISCUSSION

Our complex conductivity measurements show that the CEC of the clays is the primary factor influencing the in-phase and quadrature conductivities of clays and clay-sand mixtures with a high clay content (≥ 5% of the total volume) and that the porosity changes (through the calculation of the formation factor) are a secondary factor, except for clay-sand mixtures with a low clay content (1% of the sample volume). For these mixtures, the low-frequency complex conductivity spectra are influenced by the electrochemical conduction and polarization of clays and sands. In addition, the quadrature conductivity of smectite-rich mixtures is fairly independent of salinity because of the constant CEC of smectite. Therefore, the specific surface areas and surface charge densities associated with the different clay mineralogies control the recorded complex conductivities of clay-rich mixtures, in particular, their quadrature conductivity.

The use of our new induced polarization model confirms the importance of Stern layer polarization for the quadrature conductivities of clay-sand mixtures. The use of the Donnan equilibrium model and the volumetric excess of charge in our new induced polarization model improves considerably the calculation of the surface site densities of adsorbed ions in the Stern and diffuse layers (compared to the SIP model of Leroy and Revil, 2009). This allows the calculation of considerably higher surface site densities of ad-

Table 5. Petrophysical and interfacial parameters of our induced polarization model to describe in-phase and quadrature conductivity spectra of pure K1-clay and (K1 + S) mixtures with varying clay contents at different salinities (NaCl). S and K stand for sand and kaolinite, respectively. The values of f_Q, S_s, Q_0, and CEC are determined only for the end members. $\beta^{St}_{\mathrm{Na}^+} = \beta^{f}_{\mathrm{Na}^+}/2$.

K%	S%	C^f_{NaCl} $\mathrm{mol\,L^{-1}}$	d_{50} µm	ϕ	m	F[11]	f_Q	S_s[12] $\mathrm{m^2\,g^{-1}}$	Q_0[13] $\mathrm{C\,m^{-2}}$	CEC $\mathrm{meq\,g^{-1}}$
100	0	0.0017	120	0.55	2.1	3.5	0.95	137	−0.12	0.18
		0.017					0.97			
		0.17					0.99			
20	80	0.0017	—	0.30	1.6	6.9	—	—	—	—
		0.017								
		0.17								
1	99	0.0017	—	0.35	1.5	4.8	—	—	—	—
		0.017								
		0.17								
0	100	0.0017	208	0.35	—	4.8	0.3	0.5	−0.025	—
		0.017					0.4		−0.080	
		0.17					0.5		−0.140	

[11] F is calculated using the cementation exponent, porosity, and Archie law ($F = \phi^{-m}$).

[12] The theoretical specific surface area of K1 clay is estimated using its mineralogical composition (80% of kaolinite, 15% of smectite, and 5% of illite-muscovite, in weight percentage, Table 1) and average specific surface areas of kaolinite ($15\ \mathrm{m^2\,g^{-1}}$), smectite ($800\ \mathrm{m^2\,g^{-1}}$), and illite ($100\ \mathrm{m^2\,g^{-1}}$) reported by Revil and Leroy (2004) ($S_S = \sum_i w_i S_{Si}$).

[13] The surface charge density is calculated using $Q_0 = -10^{-3} e N_A \mathrm{CEC}/S_s$ (equation 9).

Table 6. Petrophysical and interfacial parameters of our induced polarization model to describe in-phase and quadrature conductivity spectra of pure K1-clay and (K1 + S) mixtures with varying clay contents at different salinities (NaCl). S and K stand for sand and kaolinite, respectively. The values of f_Q, S_s, Q_0, and CEC are determined only for the end members. $\beta^{St}_{\mathrm{Na}^+} = \beta^{f}_{\mathrm{Na}^+}/350$.

K%	S%	C^f_{NaCl} $\mathrm{mol\,L^{-1}}$	d_{50} µm	ϕ	m	F[14]	f_Q	S_s[15] $\mathrm{m^2\,g^{-1}}$	Q_0[16] $\mathrm{C\,m^{-2}}$	CEC $\mathrm{meq\,g^{-1}}$
100	0	0.0017	9	0.55	2.1	3.5	0.97	137	−0.93	1.4
		0.017					0.98			
		0.17					0.99			
20	80	0.0017	—	0.30	1.6	6.9	—	—	—	—
		0.017								
		0.17								
1	99	0.0017	—	0.35	1.5	4.8	—	—	—	—
		0.017								
		0.17								
0	100	0.0017	208	0.35	—	4.8	0.3	0.5	−0.025	—
		0.017					0.4		−0.080	
		0.17					0.5		−0.140	

[14] The value of F is calculated using the cementation exponent, porosity and Archie law ($F = \phi^{-m}$).

[15] The theoretical specific surface area of K1-clay is estimated using its mineralogical composition (80% of kaolinite, 15% of smectite, and 5% of illite-muscovite, in weight percentage; Table 1) and average specific surface areas of kaolinite ($15\ \mathrm{m^2\,g^{-1}}$), smectite ($800\ \mathrm{m^2\,g^{-1}}$), and illite ($100\ \mathrm{m^2\,g^{-1}}$) reported by Revil and Leroy (2004) ($S_S = \sum_i w_i S_{Si}$).

[16] The surface charge density is calculated using $Q_0 = -10^{-3} e N_A \mathrm{CEC}/S_s$ (equation 9).

Downloaded 11/18/14 to 138.67.11.98. Redistribution subject to SEG license or copyright; see Terms of Use at http://library.seg.org/

Downloaded 11/18/14 to 138.67.11.98. Redistribution subject to SEG license or copyright; see Terms of Use at http://library.seg.org/

sorbed counterions in the Stern layer (compared to a simple TLM). It seems that this ingredient is required to explain the experimental data. Indeed, if the surface site densities of adsorbed counterions in the Stern layer are fitted according to the TLM (this is done by Leroy and Revil, 2009), the modeled complex conductivities would be too low to reproduce the experimental data. Leroy and Revil (2009) also underestimate the DC surface conductivity of clays because they assume that the Stern layer does not participate to conduction currents. In addition, the fitted partition coefficient values (i.e., the ratios of the surface charge density of the Stern layer to the total surface charge density of the EDL; f_Q) are in agreement with the values computed earlier by Leroy and Revil (2009) for clays and Leroy et al. (2013) for sands. Furthermore, the coating clay model used in the present paper is also necessary to reproduce the laboratory data set of low-frequency complex conductivities of clay-sand mixtures. The SIP model of Leroy and Revil (2009) cannot be applied to clay-sand mixtures because it only considers one type of mineral and not mixtures. In addition, the use of the full DEM theory increases the magnitude of calculated conduction and polarization currents. Leroy and Revil (2009) use an analytical solution of the DEM, which is useful for low ratios of surface to bulk conductivity.

A fairly good agreement between our induced polarization model based on the Stern layer polarization and the experimental data was obtained except below 10^{-1} Hz. At these very low frequencies, the polarization mechanism may correspond to membrane polarization as mentioned by Leroy and Revil (2009) and Revil and Florsch (2010). This mechanism is associated with grain-grain interactions and occurs at larger scales (over multiple grain lengths) compared to the grain polarization mechanism investigated in our paper. This can explain why this phenomenon may occur at very low frequencies. Furthermore, the quadrature conductivities of B2-clay and B2-sand mixtures are slightly better predicted than the quadrature conductivities of K1-clay and K1-sand mixtures. Regarding the mineralogical compositions of the two clay samples (K1-clay: 80% of kaolinite, 15% of smectite, 5% of illite-muscovite; B2-clay: 95% of smectite and 5% of kaolinite in weight percentage; Table 1), B2-clay is more homogeneous than K1-clay. This can explain why the PSD and therefore the quadrature conductivity of K1-clay are more difficult to reproduce than those of B2-clay. In addition, the fitting of the quadrature conductivity tends to be poorer only for the highest salinity (0.17 mol L^{-1} NaCl) and in the case of 1% of the sample volume occupied by clay (K1 or B2). The recorded phases of these mixtures are low at the highest salinity (mostly <0.1 mrad, so below the sensitivity of the equipment). Furthermore, the modeled PSDs are significantly broader than the measured ones (with a laser granulometer in vacuum) because of the effects of particle shape and surface roughness on the complex conductivity measurements.

The last point is related to the value of the surface mobility of the counterions in the Stern layer. We tested two assumptions: (1) that the surface mobility of the sodium ion is equal to half its value in the bulk pore water (Tournassat et al.,

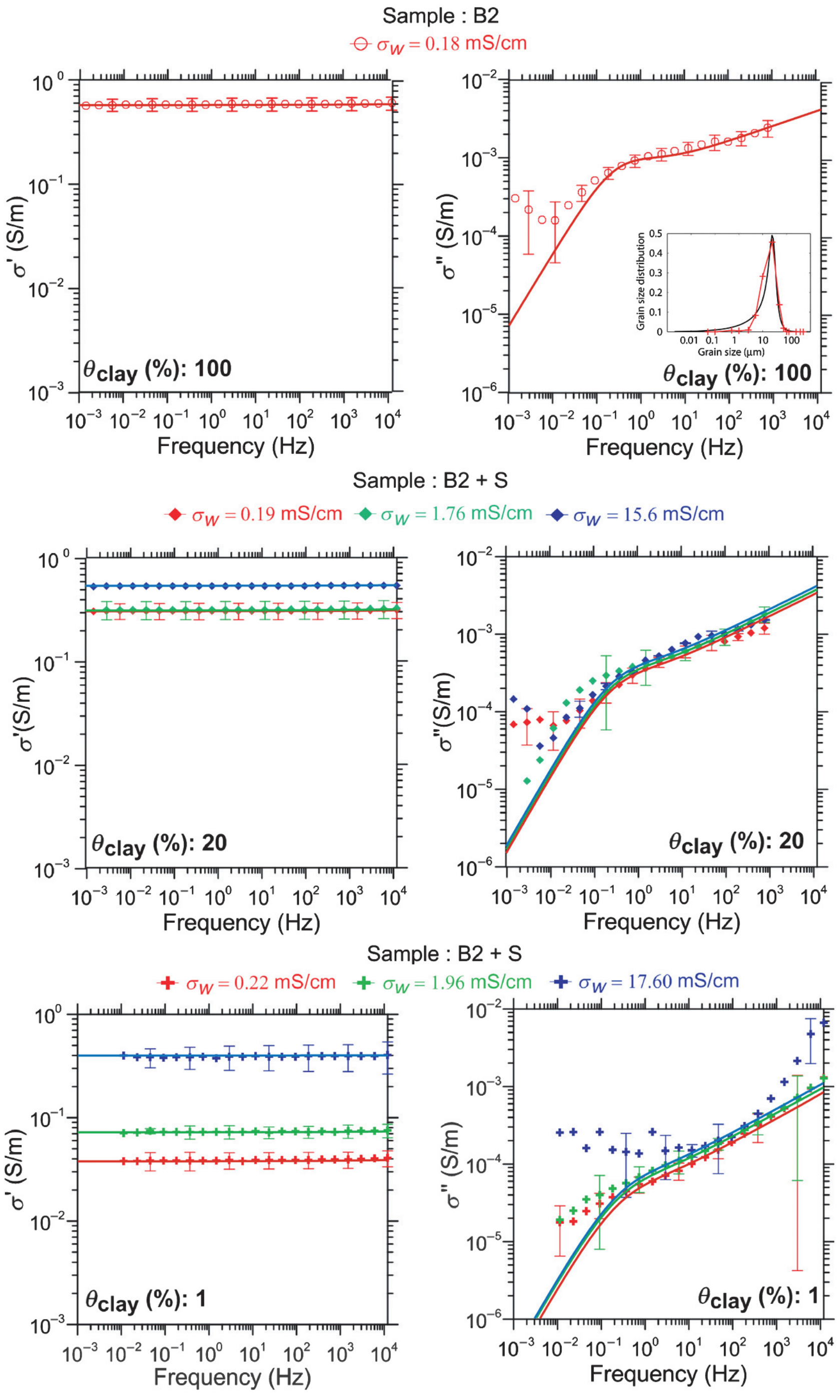

Figure 16. Modeled (lines) in-phase and quadrature conductivity spectra of clay-sand mixtures (B2 + S) for different saturating fluid salinities and clay contents (symbols: measurements). The modeled grain size distribution is represented by the black line in the upper right hand corner (symbols: measurements in vacuum).

Downloaded 11/18/14 to 138.67.11.98. Redistribution subject to SEG license or copyright; see Terms of Use at http://library.seg.org/

2009; Bourg and Sposito, 2011) and (2) that the surface mobility of the sodium ion is equal to 1/350th of its value in the bulk pore water (Revil, 2012). Predictions of complex conductivity spectra using the two assumptions give similar results, except that assumption (2) leads to smaller grain sizes and higher CEC and f_Q than assumption (1) (Tables 5–8). According to assumption (1), the Stern layers of large clay aggregates control the complex conductivity response of the samples. According to assumption (2), the Stern layers of small micrometric clay aggregates control the complex conductivity of clays and clay-sand mixtures, which appears to be for us a more realistic assumption than assumption (1).

CONCLUSION

We have developed a new experimental database regarding the dependence of the low-frequency complex conductivity of clay-sand mixtures with the clay mineralogy (kaolinite and smectite), clay content, and salinity (NaCl). The following conclusions have been reached:

1) The in-phase and quadrature conductivities increase steadily with the clay content. The quadrature conductivity is proportional to the CEC, and the CEC of a material is proportional to the clay content as long as the mineralogy stays the same.

Table 7. Petrophysical and interfacial parameters of our induced polarization model to describe in-phase and quadrature conductivity spectra of pure bentonite (B2) and (B2 + S) mixtures with varying clay contents at different salinities (NaCl). "S" and "B" stand for sand and bentonite, respectively. The values of f_Q, S_s, Q_0, and CEC are determined only for the end-members. $\beta^{St}_{Na^+} = \beta^f_{Na^+}/2$.

B%	S%	C^f_{NaCl} mol L^{-1}	d_{50} µm	ϕ	m	F[17]	f_Q	S_s m^2 g^{-1}	Q_0[18] C m^{-2}	CEC meq g^{-1}
100	0	0.0017	56	0.67	4	5	0.70	800	−0.053	0.442
		0.017					0.75			
		0.17					0.80			
20	80	0.0017	—	0.50	2	4	—	—	—	—
		0.017								
		0.17								
1	99	0.0017	—	0.55	2	3.3	—	—	—	—
		0.017								
		0.17								
0	100	0.0017	208	0.35	—	4.8	0.3	0.5	−0.025	—
		0.017					0.4		−0.080	
		0.17					0.5		−0.140	

[17] F is calculated using the cementation exponent, porosity, and Archie's law ($F = \phi^{-m}$).

[18] The surface charge density is calculated using $Q_0 = -10^{-3} e N_A \mathrm{CEC}/S_s$ (equation 9).

Table 8. Petrophysical and interfacial parameters of our induced polarization model to describe in-phase and quadrature conductivity spectra of pure bentonite (B2) and (B2 + S) mixtures with varying clay contents at different salinities (NaCl). S and B stand for sand and bentonite, respectively. The values of f_Q, S_s, Q_0, and CEC are determined only for the end members. $\beta^{St}_{Na^+} = \beta^f_{Na^+}/350$.

B%	S%	C^f_{NaCl} mol L^{-1}	d_{50} µm	ϕ	m	F[19]	f_Q	S_s m^2 g^{-1}	Q_0[20] C m^{-2}	CEC meq g^{-1}
100	0	0.0017	4.2	0.27	4	188	0.93	800	−0.053	0.442
		0.017					0.95			
		0.17					0.99			
20	80	0.0017	—	0.50	2	4	—	—	—	—
		0.017								
		0.17								
1	99	0.0017	—	0.55	2	3.3	—	—	—	—
		0.017								
		0.17								
0	100	0.0017	208	0.35	—	4.8	0.3	0.5	−0.025	—
		0.017					0.4		−0.080	
		0.17					0.5		−0.140	

[19] F is calculated using the cementation exponent, porosity, and Archie's law ($F = \phi^{-m}$).

[20] The surface charge density is calculated using $Q_0 = -10^{-3} e N_A \mathrm{CEC}/S_s$ (equation 9).

Downloaded 11/18/14 to 138.67.11.98. Redistribution subject to SEG license or copyright; see Terms of Use at http://library.seg.org/

2) The quadrature conductivity of smectite-rich materials increases only slightly with salinity except at very low clay content (1% of the sample volume). The CEC of smectite-rich materials depends on the surface charge density of smectite. The surface charge density of smectite is controlled by isomorphic substitutions in its crystalline framework and is roughly constant with salinity. The situation may be different for pure kaolinite because of the strong effect of the amphoteric sites on the edge of the crystals with a surface charge density that is salinity dependent.
3) The experimental data are successfully interpreted by an SIP model. This model combines a Donnan equilibrium model of the surface electrochemical properties of clay minerals and sand, a conduction model of the Stern and diffuse layers, a polarization model of the Stern layer, and a macroscopic conductivity model based on the full DEM theory. This induced polarization model also considers the complex surface conductivity of particles with different sizes and the combined electric response of clays and sand. Nevertheless, at very low frequencies ($<10^{-1}$Hz), our model cannot predict the quadrature conductivity. The missing polarization mechanism may correspond to membrane polarization, and efforts should be made to incorporate this contribution into a unified model.

ACKNOWLEDGEMENTS

This research was supported by the French Institute for Radioprotection and Nuclear Safety. The authors are grateful to D. Bartier and M. Blanc-Valleron for carrying out the XRD analysis and to N. Betin and A. Bouchet for the CEC analysis. The work of P. Leroy was supported by the NEEDS MIPOR Zetaclay, CAPTANDRA, Eurogia+ CO2FieldLab and Dév. Hydrogéophysiques projects. The work of A. Revil was supported by the OCLASSH Consortium. P. Leroy warmly thanks C. Tournassat and S. Grangeon for fruitful discussions. We thank the editor and the referees.

REFERENCES

Archie, G. E., 1942, Electrical resistivity log as an aid in determining some reservoir characteristics: Transactions of the AIME, **146**, 54–61, doi: 10.2118/942054-G.

Baba, J., and P. D. Komar, 1981, Measurements and analysis of settling velocities of natural quartz sand grains: Journal of Sedimentary Petrology, **51**, 631–640, doi: 10.2110/jsr.51.631.

Binley, A., L. D. Slater, M. Fukes, and G. Cassiani, 2005, Relationship between spectral induced polarization and hydraulic properties of saturated and unsaturated sandstone: Water Resources Research, **41**, W12417, doi: 10.1029/2005WR004202.

Bourg, I. C., and G. Sposito, 2011, Molecular dynamics simulations of the electrical double layer on smectite surfaces contacting concentrated mixed electrolyte (NaCl-CaCl2) solutions: Journal of Colloid and Interface Science, **360**, 701–715, doi: 10.1016/j.jcis.2011.04.063.

Bruggeman, D. A. G., 1935, Berechnung verschiedener physikalischer Konstanten von heterogenen Substanzen: Annalen der Physik, **416**, 636–664, doi: 10.1002/andp.19354160705.

Bücker, M., and A. Hördt, 2013, Analytical modelling of membrane polarization with explicit parametrization of pore radii and the electrical double layer: Geophysical Journal International, **194**, 804–813, doi: 10.1093/gji/ggt136.

Cadène, A., B. Rotenberg, S. Durand-Vidal, J.-C. Badot, and P. Turq, 2006, Dielectric spectroscopy as a probe for dynamic properties of compacted smectites: Physics and Chemistry of the Earth, **31**, 505–510, doi: 10.1016/j.pce.2006.04.002.

Cosenza, P., A. Ghorbani, C. Camerlynck, F. Rejiba, R. Guérin, and A. Tabbagh, 2009, Effective medium theories for modelling the relationships between electromagnetic properties and hydrological variables: A review: Near Surface Geophysics, **7**, 563–578, doi: 10.3997/1873-0604.2009009.

Delgado, A., F. Gonzalezcaballero, and J. M. Bruque, 1986, On the zeta-potential and surface-charge density of montmorillonite in aqueous-electrolyte solutions: Journal of Colloid and Interface Science, **113**, 203–211, doi: 10.1016/0021-9797(86)90220-1.

Donnan, F. G., 1924, The theory of membrane equilibria: Chemical Reviews, **1**, 73–90, doi: 10.1021/cr60001a003.

Dukhin, S. S., and V. N. Shilov, 1974, Dielectric phenomena and the double layer in disperse systems and polyelectrolytes: John Wiley and Sons, Inc.

Fraser, D. C., N. B. Keevil, and S. H. Ward, 1964, Conductivity spectra of rocks from the Craigmont ore environment: Geophysics, **29**, 832–847, doi: 10.1190/1.1439425.

Gazoty, A., G. Fiandaca, J. Pedersen, E. Auken, and A. V. Christiansen, 2012, Mapping of landfills using time domain spectral induced polarization data: The Eskelund case study: Near Surface Geophysics, **10**, 563–574, doi: 10.3997/1873-0604.2012046.

Grosse, C., S. Pedrosa, and V. N. Shilov, 1999, Calculation of the dielectric increment and characteristic time of the LFDD in colloidal suspensions of spheroidal particles: Journal of Colloid and Interface Science, **220**, 31–41, doi: 10.1006/jcis.1999.6486.

Hanai, T., 1968, Electrical properties of emulsions: *in* P. Sherman, ed., Emulsions science, Academic Press, 354–477.

Hassan, M. S., F. Villieras, F. Gaboriaud, and A. Razafitianamaharavo, 2006, AFM and low-pressure argon adsorption analysis of geometrical properties of phyllosilicates: Journal of Colloid and Interface Science, **296**, 614–623, doi: 10.1016/j.jcis.2005.09.028.

Holland, R., T. Günther, and U. Yaramanci, 2010, Aquifer characterisation by spectral induced polarization — Field and laboratory measurements: 16th European Meeting of Environmental and Engineering Geophysics, Extended abstract.

Holtzapffel, T., 1985, Les minéraux argileux. Préparation. Analyse diffractométrique et détermination: Société Géologique du Nord.

Hunter, R. J., 1981, Zeta potential in colloid science: Principles and applications: Academic Press.

Jackson, M. L., 1964, Soil chemical analysis: Prentice Hall, Inc.

Jimenez, M. L., and T. Bellini, 2010, The electrokinetic behavior of charged non-spherical colloids: Current Opinion in Colloid and Interface Science, **15**, 131–144, doi: 10.1016/j.cocis.2009.11.003.

Jougnot, D., A. Ghorbani, A. Revil, P. Leroy, and P. Cosenza, 2010, Spectral induced polarization of partially saturated clay-rocks: A mechanistic approach: Geophysical Journal International, **180**, 210–224, doi: 10.1111/j.1365-246X.2009.04426.x.

Kan, R., and P. N. Sen, 1987, Electrolytic conduction in periodic arrays of insulators with charges: Journal of Chemical Physics, **86**, 5748–5756, doi: 10.1063/1.452502.

Klein, D. J., and W. R. Sill, 1982, Electrical properties of artificial clay-bearing sandstones: Geophysics, **47**, 1593–1605, doi: 10.1190/1.1441310.

Knight, R. J., and A. Endres, 1990, A new concept in modelling the dielectric response of sandstones: Geophysics, **55**, 586–594, doi: 10.1190/1.1442870.

Leroy, P., N. Devau, A. Revil, and M. Bizi, 2013, Influence of surface conductivity on the apparent zeta potential of amorphous silica nanoparticles: Journal of Colloid and Interface Science, **410**, 81–93, doi: 10.1016/j.jcis.2013.08.012.

Leroy, P., D. Jougnot, A. Revil, A. Lassin, and M. Azaroual, 2012, A double layer model of the gas bubble/water interface: Journal of Colloid and Interface Science, **388**, 243–256, doi: 10.1016/j.jcis.2012.07.029.

Leroy, P., and A. Revil, 2004, A triple layer model of the surface electrochemical properties of clay minerals: Journal of Colloid and Interface Science, **270**, 371–380, doi: 10.1016/j.jcis.2003.08.007.

Leroy, P., and A. Revil, 2009, Spectral induced polarization of clays and clay-rocks: Journal of Geophysical Research, **114**, B10202, doi: 10.1029/2008JB006114.

Leroy, P., A. Revil, S. Altmann, and C. Tournassat, 2007, Modeling the composition of the pore water in a clay-rock geological formation (Callovo-Oxfordian, France): Geochimica et Cosmochimica Acta, **71**, 1087–1097, doi: 10.1016/j.gca.2006.11.009.

Leroy, P., A. Revil, and D. Coelho, 2006, Diffusion of ionic species in bentonite: Journal of Colloid and Interface Science, **296**, 248–255, doi: 10.1016/j.jcis.2005.08.034.

Leroy, P., A. Revil, A. Kemna, P. Cosenza, and A. Ghorbani, 2008, Spectral induced polarization of water-saturated packs of glass beads: Journal of Colloid and Interface Science, **321**, 103–117, doi: 10.1016/j.jcis.2007.12.031.

Leroy, P., C. Tournassat, and M. Bizi, 2011, The influence of surface conductivity on the apparent zeta potential of TiO_2 nanoparticles: Journal of Colloid and Interface Science, **356**, 442–453, doi: 10.1016/j.jcis.2011.01.016.

Lesmes, D. P., and S. P. Friedman, 2005, Relationships between the electrical and hydrogeological properties of rocks and soils: *in* Y. Rubin, and S. S. Hubbard, eds., : Hydrogeophysics: Springer, Water Science and Technology Library, vol. 50, 87–128.

Lesmes, D. P., and F. D. Morgan, 2001, Dielectric spectroscopy of sedimentary rocks: Journal of Geophysical Research, **106**, 13329–13346, doi: 10.1029/2000JB900402.

Lima, O. A. L., and M. M. Sharma, 1990, A grain conductivity approach to shaly sandstones: Geophysics, **55**, 1347–1356, doi: 10.1190/1.1442782.

Lockhart, N. C., 1980, Electrical properties and the surface characteristics and structure of clays. 1. Swelling clays: Journal of Colloid and Interface Science, **74**, 509–519, doi: 10.1016/0021-9797(80)90220-9.

Marshall, D. J., and T. R. Madden, 1959, Induced polarization, a study of its causes: Geophysics, **24**, 790–816, doi: 10.1190/1.1438659.

Mendelson, K. S., and M. H. Cohen, 1982, The effect of grain anisotropy on the electrical properties of sedimentary rocks: Geophysics, **47**, 257–263, doi: 10.1190/1.1441332.

O'Konski, C. T., 1960, Electric properties of macromolecules V. Theory of ionic polarization in polyelectrolytes: Journal of Physical Chemistry, **64**, 605–619, doi: 10.1021/j100834a023.

Olhoeft, G. R., 1981, Electrical properties of rocks, *in* Y. S. Touloukian, W. R. Judd, and R. F. Roy, eds., Physical properties of rocks and minerals, McGraw-Hill, 257–339.

Revil, A., 1999, Ionic diffusivity, electrical conductivity, membrane and thermoelectric potentials in colloids and granular porous media: A unified model: Journal of Colloid and Interface Science, **212**, 503–522, doi: 10.1006/jcis.1998.6077.

Revil, A., 2000, Thermal conductivity of unconsolidated sediments with geophysical applications: Journal of Geophysical Research, **105**, 16749–16768, doi: 10.1029/2000JB900043.

Revil, A., 2012, Spectral induced polarization of shaly sands: Influence of the electrical double layer: Water Resources Research, **48**, W02517, doi: 10.1029/2011WR011260.

Revil, A., 2013, Effective conductivity and permittivity of unsaturated porous materials in the frequency range 1 mHz–1 GHz: Water Resources Research, **49**, doi: 10.1029/2012WR012700.

Revil, A., L. M. Cathles, S. Losh, and J. A. Nunn, 1998, Electrical conductivity in shaly sands with geophysical applications: Journal of Geophysical Research, **103**, 23925–23936, doi: 10.1029/98JB02125.

Revil, A., M. Skold, S. Hubbard, Y. Wu, D. Watson, and M. Karaoulis, 2013a, Petrophysical properties of saprolites from the Oak Ridge Integrated Field Research Challenge site, Tennessee: Geophysics, **78**, no. 1, D21–D40, doi: 10.1190/geo2012-0176.1.

Revil, A., J. D. Eppehimer, M. Skold, M. Karaoulis, L. Godinez, and M. Prasad, 2013b, Low-frequency complex conductivity of sandy and clayey materials: Journal of Colloid Interface Science, **398**, 193–209, doi: 10.1016/j.jcis.2013.01.015.

Revil, A., and N. Florsch, 2010, Determination of permeability from spectral induced polarization in granular media: Geophysical Journal International, **181**, 1480–1498, doi: 10.1111/j.1365-246X.2010.04573.x.

Revil, A., and P. W. J. Glover, 1997, Theory of ionic-surface electrical conduction in porous media: Physical Review B, **55**, 1757–1773, doi: 10.1103/PhysRevB.55.1757.

Revil, A., and P. Leroy, 2004, Constitutive equations for ionic transport in porous shales: Journal of Geophysical Research, **109**, B03208, doi: 10.1029/2003JB002755.

Sahai, N., and D. Sverjensky, 1997, Solvation and electrostatic model for specific electrolyte adsorption: Geochimica et Cosmochimica Acta, **61**, 2827–2848, doi: 10.1016/S0016-7037(97)00127-0.

Schön, J. H., 2004, Physical properties of rocks: Fundamentals and principles: Petrophysics: Elsevier Science.

Schurr, J. M., 1964, On the theory of the dielectric dispersion of spherical colloidal particles in electrolyte solution: Journal of Physical Chemistry, **68**, 2407–2413, doi: 10.1021/j100791a004.

Schwarz, G., 1962, A theory of the low-frequency dielectric dispersion of colloidal particles in electrolyte solution: Journal of Physical Chemistry, **66**, 2636–2642, doi: 10.1021/j100818a067.

Sen, P. N., W. C. Chew, and D. Wilkinson, 1984, Dielectric enhancement due to geometrical and electrochemical effects: AIP Conference Proceedings**107**, 52–65.

Sen, P. N., C. Scala, and M. H. Cohen, 1981, A self-similar model for sedimentary rocks with application to the dielectric constant of fused glass beads: Geophysics, **46**, 781–795, doi: 10.1190/1.1441215.

Slater, L., D. Ntarlagiannis, F. D. Day-Lewis, K. Mwakanyamale, J. W. Lane, A. Ward, and R. J. Versteeg, 2010, Use of induced polarization to characterize the hydrogeologic framework of the zone of surface-water/groundwater exchange at the Hanford 300 Area: WA. SAGEEP, **23**, 955–960.

Sverjensky, D. A., 2005, Prediction of surface charge on oxides in salt solutions: Revisions for 1:1 (M+L-) electrolytes: Geochimica et Cosmochimica Acta, **69**, 225–257, doi: 10.1016/j.gca.2004.05.040.

Telford, W. M., L. P. Geldart, R. E. Sheriff, and D. A. Keys, 1990, Applied geophysics: Cambridge University Press.

Tombacz, E., and M. Szekeres, 2004, Colloidal behavior of aqueous montmorillonite suspensions: The specific role of pH in the presence of indifferent electrolytes: Applied Clay Science, **27**, 75–94, doi: 10.1016/j.clay.2004.01.001.

Tombacz, E., and M. Szekeres, 2006, Surface charge heterogeneity of kaolinite in aqueous suspension in comparison with montmorillonite: Applied Clay Science, **34**, 105–124, doi: 10.1016/j.clay.2006.05.009.

Tournassat, C., and C. A. J. Appelo, 2011, Modelling approaches for anion-exclusion in compacted Na-bentonite: Geochimica et Cosmochimica Acta, **75**, 3698–3710, doi: 10.1016/j.gca.2011.04.001.

Tournassat, C., M. Bizi, G. Braibant, and C. Crouzet, 2011, Influence of montmorillonite tactoid size on Na-Ca cation exchange reactions: Journal of Colloid and Interface Science, **364**, 443–454, doi: 10.1016/j.jcis.2011.07.039.

Tournassat, C., Y. Chapron, P. Leroy, M. Bizi, and F. Boulahya, 2009, Comparison of molecular dynamics simulations with triple layer and modified Gouy-Chapman models in a 0.1 M NaCl-montmorillonite system: Journal of Colloid and Interface Science, **339**, 533–541, doi: 10.1016/j.jcis.2009.06.051.

Tournassat, C., S. Grangeon, P. Leroy, and E. Giffaut, 2013, Modeling specific pH dependent sorption of divalent metals on montmorillonite surfaces. A review of pitfalls, recent achievements and current challenges: American Journal of Science, **313**, 395–451, doi: 10.2475/05.2013.01.

Turq, P., F. Lantelme, and M. Chemla, 1969, Coefficients d'autodiffusion dans les solutions aqueuses de NaF et NaCl: Electrochimica Acta, **14**, 1081–1088, doi: 10.1016/0013-4686(69)80035-6.

Vacquier, V., C. R. Holmes, P. R. Kintzinger, and M. Lavergne, 1957, Prospecting for ground water by induced polarization: Geophysics, **22**, 660–687, doi: 10.1190/1.1438402.

Vinegar, H. J., and M. H. Waxman, 1984, Induced polarization of shaly sands: Geophysics, **49**, 1267–1287, doi: 10.1190/1.1441755.

Waxman, M. H., and L. J. M. Smits, 1968, Electrical conductivities in oil-bearing shaly sands: Society of Petroleum Engineers Journal, **8**, 107–122, doi: 10.2118/1863-A.

Weller, A., and F. Börner, 1996, Measurements of spectral induced polarization for environmental purposes: Environmental Geology, **27**, 329–334, doi: 10.1007/BF00766702.

Weller, A., and L. Slater, 2012, Salinity dependence of complex conductivity of unconsolidated and consolidated materials: Comparisons with electrical double layer models: Geophysics, **77**, no. 5, D185–D198, doi: 10.1190/geo2012-0030.1.

Weller, A., L. Slater, and S. Nordsiek, 2013, On the relationship between induced polarization and surface conductivity: Implications for petrophysical interpretation of electrical measurements: Geophysics, **78**, no. 5, D315–D325, doi: 10.1190/geo2013-0076.1.

Downloaded 11/18/14 to 138.67.11.98. Redistribution subject to SEG license or copyright; see Terms of Use at http://library.seg.org/